UPPSALA UNIVERSITET

Independent Project at the Department of Earth Sciences
Självständigt arbete vid Institutionen för geovetenskaper
2019: 7

Spatial and Temporal Variations in a Perennial Firn Aquifer on Lomonosovfonna, Svalbard

Rumsliga och tidsmässiga variationer i en flerårig firnakvifer på Lomonosovfonna, Svalbard

Monika Hawrylak
Emma Nilsson

DEPARTMENT OF EARTH SCIENCES
INSTITUTIONEN FÖR GEOVETENSKAPER

Independent Project at the Department of Earth Sciences
Självständigt arbete vid Institutionen för geovetenskaper
2019: 7

Spatial and Temporal Variations in a Perennial Firn Aquifer on Lomonosovfonna, Svalbard

Rumsliga och tidsmässiga variationer i en flerårig firnakvifer på Lomonosovfonna, Svalbard

Monika Hawrylak
Emma Nilsson

Copyright © Monika Hawrylak & Emma Nilsson
Published at Department of Earth Sciences, Uppsala University (www.geo.uu.se),
Uppsala, 2019

Abstract

Spatial and Temporal Variations in a Perennial Firn Aquifer on Lomonosovfonna, Svalbard
Monika Hawrylak & Emma Nilsson

A firn aquifer is a type of englacial water storage that forms when surface meltwater fills up the pore space in the porous firn. If the retention time exceeds one year the feature is regarded as perennial. The melt and accumulation rates as well as the available pore space determine the formation and extent of the firn aquifer. Flow of water within the aquifer caused by gradients in hydraulic potential leads to redistribution of water and consequently to a change in the level of the water table. This thesis focuses on a perennial firn aquifer on the Lomonosovfonna ice field on Svalbard. Spatial and temporal variations in the depth to the water table as well as variations in reflectivity strength of the water table are analysed using data from ground penetrating radar surveys along with MATLAB and ArcGIS software tools. The results show a clear connection between surface topography, steepness of its slopes and depth to the water table. It is also proved that the depth varies between different years. During the four years of study, the water table in the area rose closer to the surface. The results also show that the reflections from the top of the water table are stronger and more frequently detected in areas with gentler water table slopes. A similar correlation is true for the surface topography slope, where a gentler slope shows a stronger reflectivity. The results support the previous research done on Holtedahlfonna's aquifer on Svalbard as well as aquifers on Greenland.

Key words: perennial firn aquifer, ground penetrating radar, Svalbard, Lomonosovfonna.

Independent Project in Earth Science, 1GV029, 15 credits, 2019
Supervisors: Sergey Marchenko and Rickard Pettersson
Department of Earth Sciences, Uppsala University, Villavägen 16, SE-752 36 Uppsala (www.geo.uu.se)

The whole document is available at www.diva-portal.org

Sammanfattning

Rumsliga och tidsmässiga variationer i en flerårig firnakvifer på Lomonosovfonna, Svalbard
Monika Hawrylak & Emma Nilsson

En firnakvifer är en typ av englacial vattenlagring som formas när smältvatten från en glaciärs yta fyller upp porutrymmen i porös firn. När retentionstiden överskrider ett år betraktas akviferen som flerårig. Smält- och ackumulationshastigheten samt det tillgängliga porutrymmet avgör bildningen och utsträckningen av akviferen. Vattenflödet i akviferen orsakad av gradienter i hydraulisk potential leder till omfördelning av vattnet och därmed till förändringar i vattenytans nivå. Denna uppsats fokuserar på en akvifer på isfältet Lomonosovfonna på Svalbard. De rumsliga och tidsmässiga variationerna i djupet till vattenytan samt de rumsliga variationerna i reflektivitetsstyrkan från vattenytan analyseras med hjälp av georadarmätningar samt MATLAB- och ArcGIS-mjukvaror. Resultaten visar ett tydligt samband mellan yttopografin, dess lutning samt djupet till vattenytan. Dessutom är det bevisat att djupet varierar mellan olika år. Under den fyra år långa undersökningssperioden har vattenytan i mätområdet stigit. Vidare visar resultaten att reflektioner från vattenytan är starkare och mer frekvent observerade i områden där vattenytans lutning är svag. En liknande korrelation gäller också för yttopografin, där svagare lutning ger upphov till en starkare reflektivitet. Resultaten stödjer den tidigare forskningen gjord både på akviferen på Holtedahlfonna på Svalbard och akviferer på Grönland.

Nyckelord: flerårig firnakvifer, georadar, Svalbard, Lomonosovfonna.

Självständigt arbete i geovetenskap, 1GV029, 15 hp, 2019
Handledare: Sergey Marchenko och Rickard Pettersson
Institutionen för geovetenskaper, Uppsala universitet, Villavägen 16, SE-752 36 Uppsala (www.geo.uu.se)

Hela publikationen finns tillgänglig på www.diva-portal.org

Table of Contents

1.Introduction 1
1.1 Objective 1
1.2 Background 1
1.2.1 Glaciers 1
1.2.2 Glacial hydrology 3
1.2.3 Previous studies on perennial firn aquifers 2
1.2.4 Ground penetrating radar 6
1.3 Site description 8
2. Method 10
2.1 Radar 10
2.2 Water table variations 13
2.3 Estimation of reflectivity 13
3. Results 16
3.1 Water table variations 16
3.2 Estimation of reflectivity 23
4. Discussion 27
4.1 Water table variations 27
4.2 Estimation of reflectivity 28
4.2.1 Reflectivity dependence on water table slope 28
4.2.2 Reflectivity dependence on surface topography slope 28
4.2.3 Reflectivity dependence on elevation 29
4.3 Joint discussion 29
5. Conclusions 30
Contributions 31
Acknowledgements 31
References 32

1.Introduction

1.1 Objective

Perennial firn aquifers (PFA) are a relatively new discovery when it comes to exploration of the Arctic. More so, the research is mostly focused on the aquifers of the Greenland Ice Sheet. However, firn aquifers are also present in the glaciers of the Svalbard archipelago, which has started to get more attention in recent years. This project focuses on a rather small aquifer located on the Lomonosovfonna ice field on Spitsbergen, the biggest island of Svalbard, and is a part of an ongoing unpublished research project conducted by glaciologists at the Department of Earth Sciences at Uppsala University (Sweden) and University of Utrecht (The Netherlands).

This thesis is divided into two individual subprojects working on the same dataset. Project 1 focuses on temporal and spatial variability in the depth and absolute elevation of the water table as well as understanding these variations in relation to surface topography, slope of the surface topography and the water table. Project 2 aims to derive the reflectivity of the PFA roof, explain its spatial variability, and understand the characteristics of the water flow in the glacier.

A firn aquifer forms when surface meltwater percolates through the snow and firn and fills up the pore space available in the porous firn. The discharge rates (Christianson *et al.*, 2015), the amount of meltwater produced at the surface of the glacier together with the available pore space, which is determined by the net accumulation rate, will determine the level of the water table in the aquifer (Kuipers Munneke *et al.*, 2014). Redistribution of the water and change in water table depth below the surface is a result of flow dynamics, such as lateral flow, within the aquifer (Christianson *et al.*, 2015).

In this study we hypothesize that the flow of water will show a correlation with the surface terrain. It is expected to observe a shallow water table in topographic depressions of the study area. It is also expected to observe temporal variations during the study period.

1.2 Background

1.2.1 Glaciers

The premise under which a glacier forms is that precipitation in the form of snow, hail, frost, and rain accumulates and transforms into ice through compaction during multiple years. The accumulated mass is then transported towards lower elevations. For a glacier to form it is also necessary that the input to the accumulation zone exceeds the mass loss of ice in the ablation zone (Bennett & Glasser, 2009; Benn & Evans, 2010).

A glacier may be divided into two areas, the accumulation zone where annual mass accumulation is greater than annual mass loss through ablation and the ablation zone where the ablation is greater than the accumulation. The imaginary line where accumulation equals ablation is called the equilibrium line. The amount of accumulation in relation to the amount of ablation is defined as the mass balance of the glacier. During summer, ablation is more prevalent while the same is true for

accumulation during the colder winter period. If the annual mass balance, also called the net balance, is zero, the size of the glacier will remain the same. If the net balance is negative, the ablation is larger than the accumulation and the glacier will withdraw, whereas a positive net balance results in a growing glacier (Bennett & Glasser, 2009; Benn & Evans, 2010).

Glaciers can be classified as cold glaciers, meaning that they are below the melting point, and temperate glaciers, which mainly hold a temperature at the melting point. If the glacier contains both cold and temperate ice it is called a polythermal glacier (Benn & Evans, 2010). Typical for Svalbard glaciers is that the near-surface ice in the ablation zone is cold but the accumulation area is temperate, except for the upper 10 m which are frozen during the winter (Van Pelt *et al.*, 2012).

1.2.2 Glacial hydrology

Water is present in glacial areas not only in its frozen state as ice, firn or snow but also in its liquid state. Substantial amounts of liquid water can be found in surface streams (supraglacially), between the ice and the bed (subglacially) and flowing through the glacier (englacially). It is essential to have some insight into certain hydrological concepts in order to understand the basics of glacial hydrology.

Although meltwater usually moves through a glacier quite efficiently, some of it may be contained within, on the surface, or beneath a glacier which leads to a delay in release of the runoff. The efficiency of water movement depends on the nature of the transport paths, amount of produced meltwater and the storage availability. Thus, glacial meltwater runoff varies in space and time. The path which meltwater can take while moving through or beneath a glacier is mainly controlled by two factors, hydraulic potential and resistance to flow (Benn & Evans, 2010).

The flow of water through or on a medium can be described by the gradients in the hydraulic potential, also known as hydraulic head. While the hydraulic potential of the surface streams is defined only by elevation and water's mass, to define a flow of water within or beneath a glacier the pressure factor needs to be accounted for. The hydraulic potential can be expressed by the following equation:

$$\Phi = \rho_w g z + P_w$$

where Φ is the hydraulic potential, ρ_w is water density, g is the gravitational acceleration, z is elevation, and P_w is water pressure. In the equation above, the first term on the right is called elevation head and the second term is called pressure head (Benn & Evans, 2010).

When there are no gradients in the hydraulic potential, the water is in hydrostatic equilibrium and will not flow from one place to another. Variations in hydraulic potential are induced by changes in water pressure that in turn are caused by spatial variations in water supply. When water flows through narrow passages such as a crack or a pipe, the friction that arises between the walls and the water partially supports the weight of the water. This results in a pressure drop, also called head loss (Benn & Evans, 2010).

Some important factors to consider when it comes to the flow path are the availability and variations in pore space creating flow pathways through the firn. The resistance to fluid flow through a permeable medium is described as hydraulic conductivity or permeability, both of which are connected and decrease when the flow resistance increases. Flow of water through porous media is described by Darcy's Law and is expressed by the equation below:

$$q = \frac{-\kappa}{\mu}\frac{d\Phi}{dL}$$

The relationship expressed in this equation proves that flow rates increase with both increased hydraulic gradient and permeability. It can therefore be concluded that water moves from high hydraulic gradient to low (Benn & Evans, 2010).

In a porous medium, the capacity to store liquid water decreases as the medium's density increases. Waterflow through a glacier is expressed in terms of primary and secondary permeability, representing permeability of intact snow or ice and permeability corresponding to fractures and other flow paths respectively. While intact ice is considered impermeable with its permeability of 10^{-18} m^2, snow and firn are much more porous, with their permeabilities varying between 10^{-9} m^2 and 10^{-10} m^2. Such high values lead to meltwater being able to easily penetrate into and through snow aquifers and firn aquifers (Benn & Evans, 2010).

1.2.3 Previous studies on perennial firn aquifers

Formation of a firn aquifer is a complex process that requires certain conditions. This chapter aims to present these requirements, along with background research on this topic.

Firn aquifers, that are a form of englacial water storages, are a widespread, although not yet well-understood phenomenon in the glaciers of the Arctic as well as in high altitude glaciers. Formation of such an aquifer depends on glacial meltwater and the path it takes as runoff. One of the pathways for meltwater is the vertical percolation through the upper layers of a glacier, covered by porous firn. The water may refreeze if the temperature in the snowpack is subfreezing, forming ice lenses within the firn. The latent heat released in this process will steadily warm up the snowpack. This process may lead to warming of the entire snowpack above the melting point, which in turn terminates the refreezing process. This eventually may lead to accumulation of liquid water in pore spaces and formation of a firn aquifer. The retention time depends on many factors and varies between different aquifers, which determines whether an aquifer can be regarded as perennial (Benn & Evans, 2010).

An aquifer becomes a perennial feature only when the firn remains saturated during the winter season and persists until the next year. The formation and size of such an aquifer is determined by a few interconnected factors, e.g. melt and accumulation rates and refreezing of the water. Refreezing decreases the amount of pore space between the firn grains where the water can be stored, thus affecting the amount of liquid water in the aquifer (Kuipers Munneke *et al.*, 2014). Studies have

shown a direct correlation between high air temperatures and amount of liquid water stored in the firn aquifer (Koenig *et al.*, 2014; Kuipers Munneke *et al.*, 2014).

Results from a firn aquifer modelling run by Kuipers Munneke *et al*. (2014) show that formation of a PFA coincides with high mean annual surface temperatures which in turn coincide with high melt rates. The existence and size of a PFA is hence dependent on the extent of the surface melt. Higher melt rates are associated with more water stored in the aquifer. This relationship is also established by studies on an aquifer in southeast Greenland conducted by Koenig *et al*. (2014). Their results indicate a direct correlation between surface melt rates and the depth to the water table. A significant (~1 m) rise in the surface of the water table along with a significant lowering of this surface (~2 m) was observed after a particularly hot summer (Koenig *et al.*, 2014).

Another important formation factor is the rate of accumulation. According to Kuipers Munneke *et al*. (2014), higher accumulation rates are directly correlated to higher amount of water stored for a given mean annual surface temperature and annual cycle of surface temperature. However, this is only true up to a certain accumulation rate after which this relationship is reversed. In that situation, a higher accumulation rate means lower amount of liquid water stored. This indicates a direct relationship between the accumulation rate and the pore space available for the liquid water to fill (Kuipers Munneke *et al.*, 2014).

The water stored in PFAs, with the temperature at the melting point, makes them significant heat reservoirs. Additionally, these water storages close to the surface are a relatively dark feature with albedo lower than the surrounding snow. This indicates that the response to climate changes will vary between firn aquifer regions and non-aquifer regions (Koenig *et al.*, 2014). Another effect that is currently observed is the impact of the PFAs on the glacial mass balance.

The PFAs occur both as confined and unconfined features. The water table topography of an unconfined aquifer generally follows the surface topography, appearing like a smoother version of the latter. This is a result of the flow being driven by gravity and hence gradients in the hydraulic potential. Furthermore, this feature prompts meltwater to gather in topographic depressions where slopes are very gentle, which in turn brings the water table closer to the surface in these areas. Analogously, high surface topography and hence steeper slopes lead to thinning of the water table in the saturated zone, leading to the water table appearing deeper beneath these steep areas (Christianson *et al.*, 2015).

As aforementioned, the research on the PFAs on Svalbard is not yet particularly extensive. Christianson *et al.* (2015) provide an insight into a PFA in Holtedahlfonna polythermal glacier in northwestern Svalbard. Until recently, the Holtedahlfonna glacier system was almost in balance but from 1995 the surface mass balance became negative. The primary reason for that is the increase in melt rates during the summer season. In their study, Christianson *et al.* (2015) focus on a body of water found in a depression in the glacier that was investigated with ground penetrating radar. This feature is perennial, and it is proven to exist since at least 1992. Their results show that this aquifer is unconfined, it recharges with summer meltwater and

drains during the winter. Additionally, they show a clear correlation between gradients in hydraulic potential and the slope of the water table. Because their survey area lacks large local discharge points, such as crevasses or moulins, it is suggested that meltwater that does not refreeze flows along the aquifer until it reaches the firn limit (Christianson *et al.*, 2015).

The way in which water stored in PFAs discharges is debated. The flow path of the water has a varying impact on the dynamics of the glacier as well as other factors such as sea level rise. Two main ideas regarding the connection of the PFA to the hydrologic network exist: 1) PFAs lack a connection to the englacial and subglacial hydrologic networks, and 2) the water discharges directly through englacial or subglacial hydrologic networks. Earlier research done on PFAs on Greenland supports the hypothesis that there is no connection between the aquifer and the englacial and subglacial hydrologic networks. Measurements of available pore space and height of the water table made by Koenig *et al.* (2014) showed that the very warm melt season in 2012 led to a significant rise of the water table. This implies that the water is stored in the available firn pore space rather than discharging from the aquifer continuously. The discharge of water would instead happen all at once when a threshold is met (Koenig *et al.*, 2014). In this scenario, the water would not reach the englacial or subglacial hydrological systems due to a lack of connection to them, which would reduce or eliminate the impact of surface meltwater on the ice dynamics. The catastrophic releases of firn aquifer water could however impact sea level rise, if the flow path is connected to the ocean (Koenig *et al.*, 2014; Kuipers Munneke *et al.*, 2014).

Contradictory, more recent research on Greenland supports the idea that aquifers are directly connected to the englacial and subglacial hydrological system, implicating that the meltwater may reach the bed and therefore influence ice dynamics (Miège *et al.*, 2016; Poinar *et al.*, 2017; Miller *et al.*, 2018). Radargrams from a part of a firn aquifer that lies close to areas with crevasses lack the bright reflectors which would indicate a water table, implying that the water possibly discharged into the crevasses (Miège *et al.*, 2016). Furthermore, measurements of the flow of water within the aquifer done by Miller *et al* (2018) show that the water would likely discharge, since limitations in the amount of unsaturated firn at the test site would not allow storage of all the water and no surface discharge was observed. It is therefore likely that the drainage of firn aquifer water would be connected to englacial or subglacial hydrologic networks, such as crevasses (Miller *et al.*, 2018). This is further consolidated through the work of Poinar *et al* (2017), whose model supported the theory that the firn aquifer in southeastern Greenland drained water to an area of crevasses that lied downstream. It was also shown that the water from the PFAs was enough to widen and eventually hydrofracture the crevasses to the bed, allowing meltwater to reach the subglacial hydrologic system (Poinar *et al.*, 2017). The transportation of water to the base of the ice sheet influences the ice dynamics. Water can act as a lubricant, which speeds up the movement of the ice leading to an increase in the discharge to the ocean (e.g. Van Pelt *et al.*, 2018). Surface meltwater alone is not enough to hydrofracture crevasses, meaning that a lack of firn aquifers

would hinder transportation of water to the bed. The water would instead refreeze in these crevasses (Poinar *et al.*, 2017).

However, firn aquifers in different locations discharge water in varying ways. Work done by Christianson *et al.* (2015) on Holtedahlfonna on Svalbard showed that the meltwater did not drain into crevasses or moulins due to an impermeable firn-ice transition. Instead, the discharge happened through flow of water along the aquifer until the firn ended (Christianson *et al.*, 2015). Consequently, it is crucial to study the drainage of water specifically in the firn aquifer in Lomonosovfonna to be able to draw any conclusions about its specific water discharge.

1.2.4 Ground penetrating radar

Radar can be used to investigate a variety of glacial properties such as ice thickness, structures within the ice, basal features, and hydrology (Plewes & Hubbard, 2001). The principle of a radar system is the transmission and reception of electromagnetic waves. These waves penetrate the ice and snow and as they propagate down, they are eventually either absorbed, scattered, or reflected towards the surface. The reflected signal along with the direct airwave is picked up by the receiver at the surface. Reflectivity can be described as the strength of the radar energy that is reflected to the receiver. The signal propagation in ice is affected by the properties permittivity and electrical conductivity. The depth of the reflector is associated with the signal's two-way travel time and the velocity with which the radar wave propagates through the medium (Plewes & Hubbard, 2001).

When reflected, ice penetrating radar distinguishes between different materials due to their difference in permittivity in relation to the permittivity of ice. For example, a layer of water within the ice would produce a distinct signal since the permittivity of pure water, $\varepsilon_{water} = 81$, is high relative to the permittivity of pure monocrystalline ice, $\varepsilon_{ice} = 3.2$. This relationship also produces a so-called phase polarity reversal of the reflected signal due to that the signal starts to travel at a slower speed. Another phenomenon that occurs is refraction, which is when the waves are obliquely deflected because of a change in the medium. The refraction slightly changes the direction of travel of the signal but allows energy of the signal to be transferred to deeper layers (Plewes & Hubbard, 2001).

One thing that must be taken into account when analysing the radar signal is the loss of strength in the signal as it travels through the medium, called attenuation. One factor behind the signal attenuation is scattering, which means that energy is lost due to reflection and refraction away from the direction of the receiving antenna at the surface. The reflection from the target is wanted, but reflection from other material, as well as refraction, will create the signal attenuation. Another factor behind the attenuation is spherical spreading, which means that the energy output from the radar is spread out over a spherical surface which increases with depth (Fig. 1). A third factor contributing to attenuation is that the material itself absorbs some of the energy, which is transferred to internal energy (heat).This results in energy loss related to the travel distance from the radar wave source (Plewes & Hubbard, 2001).

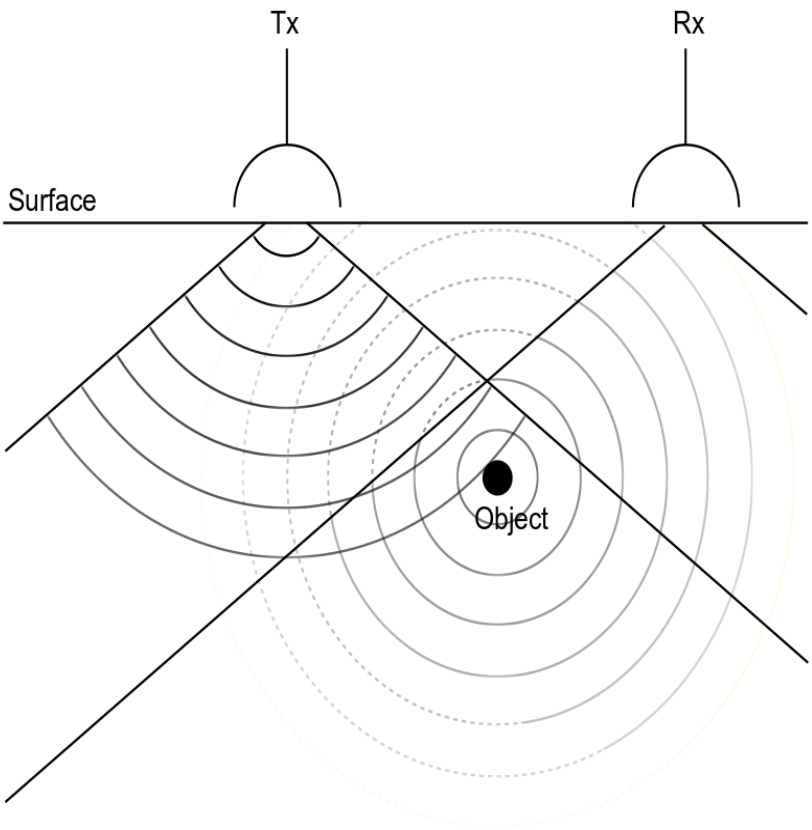

Figure 1. Spherical spreading, where Tx is the transmitter and Rx is the receiver. Image created by and republished with permission from Rickard Pettersson (Uppsala University).

1.3 Site description

The Svalbard archipelago is situated at latitude 77° to 80°N by the northern end of the Norwegian Current, an extension of the Gulf Stream. This explains Svalbard's mild climate in relation to its high latitude. The precipitation in Svalbard is quite low and varies with altitude, meaning that more precipitation will occur in e.g. the mountains compared to coastal areas (Bennett & Glasser, 2009).

During the last few decades temperature and precipitation have increased in the Arctic (Intergovernmental Panel on Climate Change, 2013). The average air temperature over the years 2015–2018 as measured by Pyramiden weather station (78°65'57''N, 16°36'03''E) is above 0°C in June-September, and below 0°C the rest of the year. The minimum average temperature is -11.4°C in March (Fig. 2).

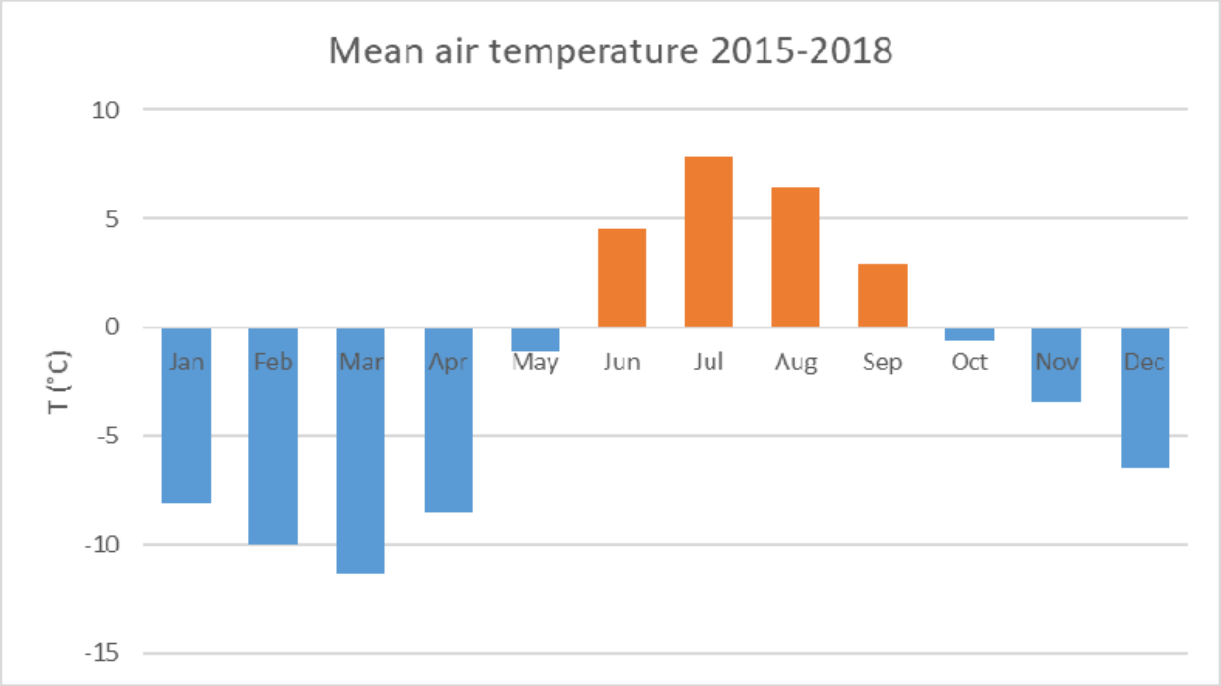

Figure 2. The mean air temperature at the weather station *Pyramiden* (°C). The maximum average temperature is 7.9°C (July) and the minimum average temperature is -11.4°C (March). Data provided by the ©Norwegian Meteorological Institute.

The aquifer studied in this project is situated on the Lomonosovfonna ice field. Lomonosovfonna lies on Spitsbergen, which is the biggest island of Svalbard. The location of Lomonosovfonna in relation to Svalbard, along with the study site where the radar data was collected, can be seen in Fig. 3. The altitude interval on Lomonosovfonna is 0–1,200 m a.s.l. and the study site lies at ~1,000 m a.s.l. Consequently, the conditions at the study site will be different than those observed at Pyramiden. This is due to adiabatic temperature decrease with elevation which means that the air temperature at the study site will be considerably lower.

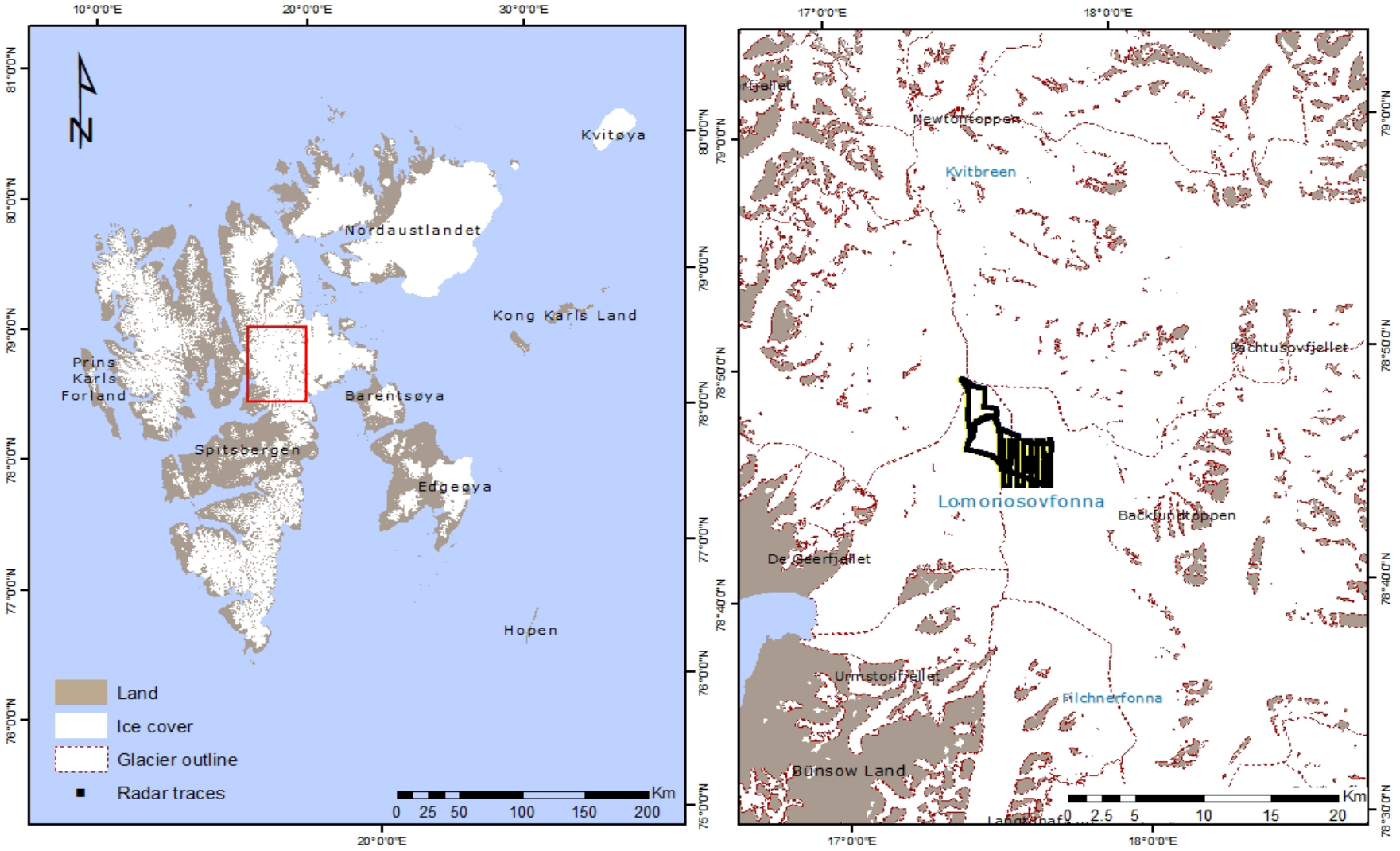

Figure 3. Map showing the location of Lomonosovfonna ice field on Svalbard. Black lines represent the traces where the ground penetrating radar survey was performed. Data provided by ©Norwegian Polar Institute and Koenig & Nuth (2010).

2. Method

2.1 Radar

The radar data covers the period 2015–2018 and was collected each year during field campaigns conducted by the Uppsala University's glaciology group. The site was surveyed during four years in different areas and each area was divided into different profiles (Fig. 4). It is important to note that different parts of the study area were surveyed in different years.

Figure 4. The area surveyed with GPR. The background shows surface topography expressed in terms of steepness of the slopes, where lighter colours indicate gentler slopes and darker colours indicate steeper slopes. The shaded relief DEM in the background provided by the ©Norwegian Polar Institute.

The radar system used in the surveys was Malå Geoscience ProEx impulse GPR system with the antenna center frequency at 250 MHz. This frequency was accurate for this survey since it assures good depth of penetration as well as reasonable

resolution, meaning that detailed radargrams can be acquired. A differential two frequency geodetic GPS (Trimble R7 GNSS) was mounted at the sled being towed by a snowmobile, along with the radar antenna and recording unit (Fig. 5). The sampling speed was 2 traces per second and the travelling speed of the snowmobile was ~10 km/h which together gave trace spacing of ~1.4 m.

Figure 5. The setup of the radar equipment during field measurements, with the snowmobile (left) and the sled with the antenna (right) that is being dragged behind. Photos by Rickard Pettersson.

The raw radar data was preprocessed beforehand by one of the supervisors and consisted of 20 files that could be further processed in MATLAB. The preprocessing included zero-time adjustment, high-pass filter, and a linear gain function. Radar surveys also provided GPS data for positioning in order to produce a map overview of the study site in ArcMap together with Digital Elevation Model (DEM) provided by Norwegian Polar Institute (NPI). Map projection Transverse Mercator and coordinate system ETRS 1989 UTM Zone 33N were used to produce all the maps in this thesis.

The dataset for the initial data processing was the same for both projects. The first step was to digitise the radargrams in MATLAB by using a tool called *pick* designed by one of the supervisors. Running the tool on each radargram allowed editing that radargram by manually drawing a line along the presumed water table. The assumption about the water table location was based on locating a bright reflector crosscutting the stratigraphic parallel snow layers. According to studies, it is plausible that such a reflector depicts the interface between wet and dry firn, i.e. the water table of the aquifer (Christianson *et al.*, 2015).

Example of a radargram can be seen on Fig. 6 while Fig. 7 shows an example of the same radargram with picked data. The parallel lines visible on the radargram represent the layers of snow. The lines that clearly deviate from the internal stratification of the firn were presumed to indicate the surface of the water table and data was picked as precisely as possible along these lines. While picking, the aim was to keep picking data points on the first break of the reflection.

Since the same process was done by both students on the same data set, it was possible to compare the results in order to obtain an estimate of error due to subjective picking of the water table in the radargram. This was done by creating a

scatterplot showing the depth in meters corresponding to the picks, with one person's picks on the x-axis and the other on the y-axis.

The data processing that followed the initial work in MATLAB differed between the two projects. The next two chapters describe the working process behind each project separately.

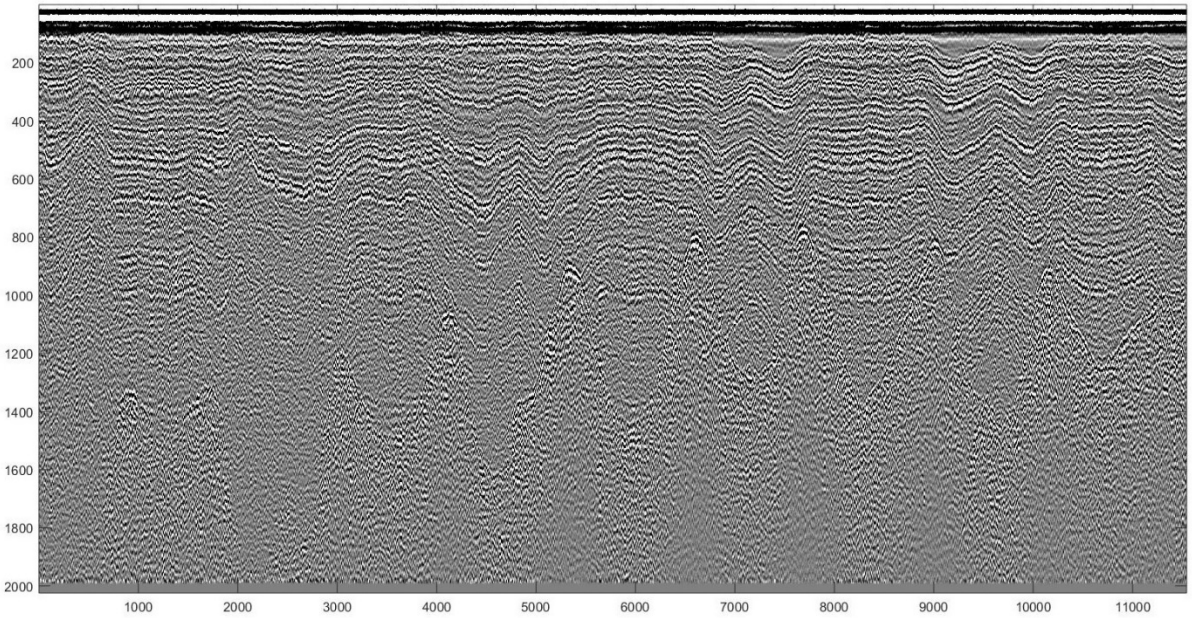

Figure 6. An example of a radargram ready to digitise in MATLAB.

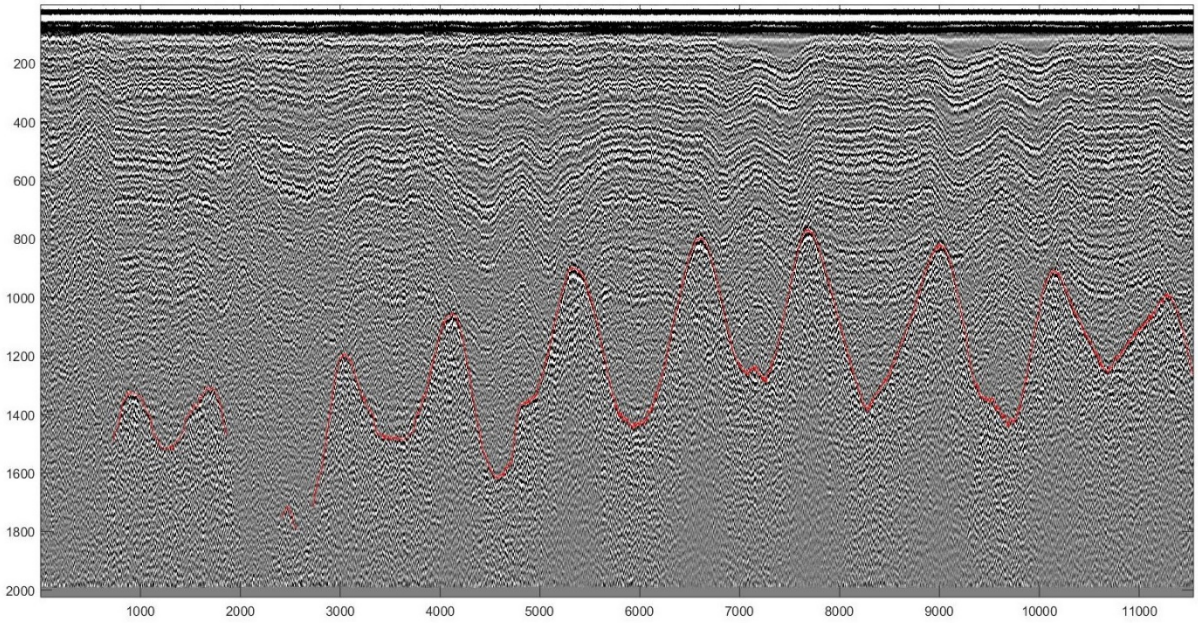

Figure 7. An example of a digitised radargram with the presumed water table traced.

2.2 Water table variations

The data acquired from digitising the radargrams was used in another tool in MATLAB, called *compilepicks*. The purpose of this tool was to compile all the output from the manual picking into one file. The output file from that was used in yet another tool, called *xover*, made to find the intersection points between the different profiles. Both tools were developed by one of the supervisors.

The output file of *xover* was a CSV file showing detailed information about profiles intersecting in a particular point. The information included e.g. profile IDs, differences in depth of the PFA roof between these two profiles, depth of the PFA roof of one of the compared profiles and depth of the PFA roof of the second compared profile. This file was prepared for further use by removing the rows with data which add no data at the crossing point (marked as *NaN*, Not a Number).

The output of the *compilepicks* tool was also a CSV file with information about all chosen traces, displayed as a table. This file also included a significant number of *NaN* values in the columns *depth* and *twtt* (two-way travel time). Rows including these values were not valuable for further examination and were manually removed in order to make the CSV file smaller and therefore easier to process in the next steps. This decreased the number of rows from ~120,000 to ~84,000. As the file was still too difficult to process for ArcMap, another tool was used to subsample the file. Running the tool decreased the data amount to ~17,000 rows which made it possible to process in ArcMap. This tool was also developed by one of the supervisors.

The outputs of both tools, subsampled *compilepicks* and *xover*, were imported into ArcMap. All data points have spatial coordinates assigned to them which made it possible to display all the points on the map in adequate places. The CSV file were converted into ArcMap *shapefiles* in order to make them editable.

These two shapefiles along with a DEM provided by Norwegian Polar Institute were then used to produce a variety of maps displaying e.g. variations in depth to the water table and topography of the study site.

The slope of the water table was constructed by first calculating the *hydraulic head* in the subsampled *compilepicks* shapefile. This calculation was done by subtracting the value of the depth to the water table from the value of the surface elevation. Then, the surface of the water table was derived by using the *Interpolation* tool, interpolating by *natural neighbors*. The output of this tool was then used as an input in the *slope* tool. The resulting output was the slope of the water table which was further used in project 2.

2.3 Estimation of reflectivity

The digitised data was further processed in MATLAB using scripts provided by the supervisors. The objective was to correct for depth, so that the extracted reflectivity values along the picked water table would depend solely on the medium from which the radar signal was reflected and not on other factors such as scattering and spherical spreading created when the signal travels through the firn.

The reflectivity is determined as the squared sum of amplitude of the signal over the reflection wavelet. To be able to determine the integration length the GPR profiles

were analysed to get the average width of the water table reflection. This was done by selecting points at the top and bottom of the reflection in seven randomly selected profiles. From each profile approximately 10 points were chosen, and the coordinates of the selected points were obtained. The coordinates from the bottom of a reflection were subtracted from the corresponding top coordinates to obtain the width at that point. All the values were used to calculate the mean width, which equals 36 (denoted as number of samples).

The amplitudes were extracted along the water table reflection that had no *gain* function applied, as *gain* will alter the reflectivity. In order to adjust for variations in the output power from the radar, the compiled reflection strength of the water table was normalised against the direct-wave amplitude of the individual traces. Finally, the attenuation with depth of the signal created when it travels through the firn was considered. This was done by estimating the attenuation rate with depth from a plot of all reflectivity values versus depth, since the amount of attenuation depends on the travel distance of the signal.

The power (Pc) plotted as a function of depth (h), with removed outliers can be seen in Fig. 8. The slope of a linear fit to the data yielded values for the attenuation rate, $a_{slope} = -1.213\ dB/km$ and $a_{offset} = 66.07\ dB$.

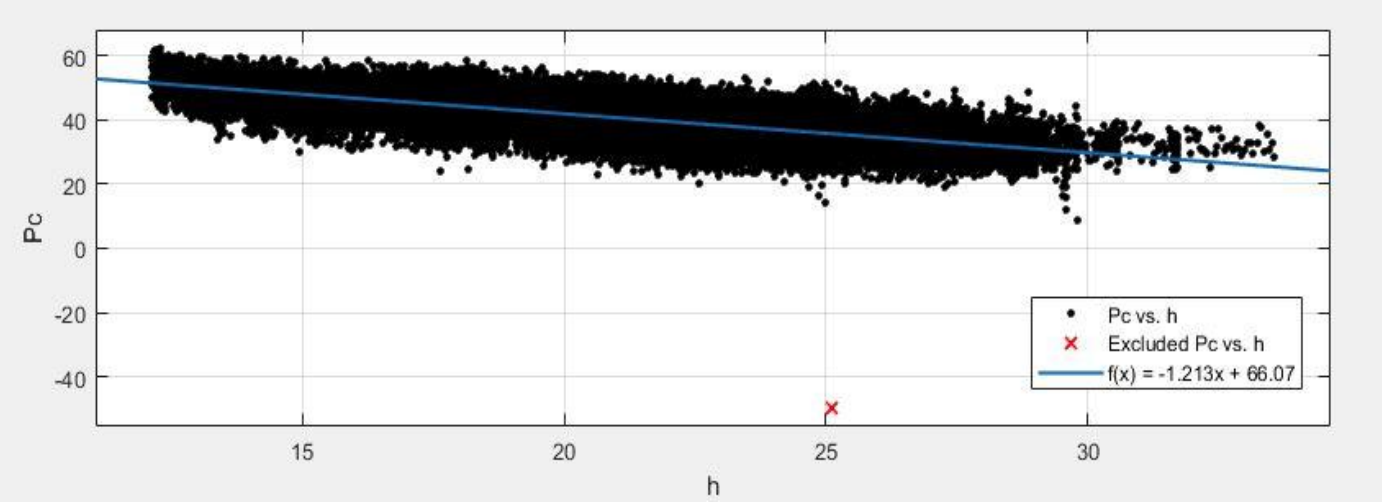

Figure 8. Power plotted as a function of depth to the water table, along with the linear fit to the data.

In the resulting reflectivity data, there also existed values that did not contain any reflectivity (*NaN*). A copy of the file was created, where all the rows with *NaN*s in the reflectivity column were deleted.

The file containing the traces both with and without reflectors, henceforth referred to as *All traces*, was imported to ArcMap as XY data. The spatial coordinates associated with the data points allowed for the traces to be projected onto a DEM downloaded from the Norwegian Polar Institute. The XY data was converted to a shapefile. The same procedure was then applied to the CSV file which only contained the traces with reflectors, *Only reflectors*.

The slope of the surface topography was extracted using the DEM. The surface slope in the study area was then correlated to the reflectivity data by first using the shapefile containing *All traces* and then using the shapefile with the reflection traces. The results were exported as CSV files before they were imported to MATLAB. Here, a histogram was created with the surface topography slope on the x-axis and number of points (representing the reflectivity) on the y-axis. Both datasets (*All traces* and *Only reflectors*) were plotted in the same histogram.

The slope of the water table was obtained from processing in project 1. This was then correlated to *All traces* and *Only reflectors* respectively. The results were exported to a CSV file and imported into MATLAB and a similar histogram as the one correlating surface topography slope with reflectivity was created, but with the water table slope on the x-axis.

Lastly, the elevation was extracted from the DEM before it was first correlated to *All traces* and then to *Only reflectors*. The CSV file was used to plot a histogram with number of points on the y-axis and the elevation on the x-axis.

To further consolidate the result as well as to analyse the difference in range of the reflectivity, two scatter plots were created: one showing the reflectivity versus the water table slope and the other showing the reflectivity versus the surface topography slope. To represent the trend of the data, a line was fitted to the maximum values using bins, which can be explained as dividing the data into intervals. When plotting both water table slope and surface topography slope the number of bins used was set to 10. For the water table slope-plot, the bins were distributed to favour the slopes lower than 4°, since most of the points were located there. The reflectivity values denoted as maximum in the surface topography slope plot were the top 0.3% values, which represents 3 standard deviations ($3\sigma = 99.7$). For the water table slope plot, the very maximum values were used.

3. Results

When comparing the digitised radargrams, the obtained correlation coefficient was $R = 0.9923$ (Fig. 9). Calculated standard deviation was $\sigma = 0.45$ and the average difference in depth to the water table between the two sets of picks was approximately 9.7 cm. The correlation between the picks in the two sub-projects follows the line representing a perfect positive correlation closely for low values, but deviates around $y = 19$ and $y = 24$.

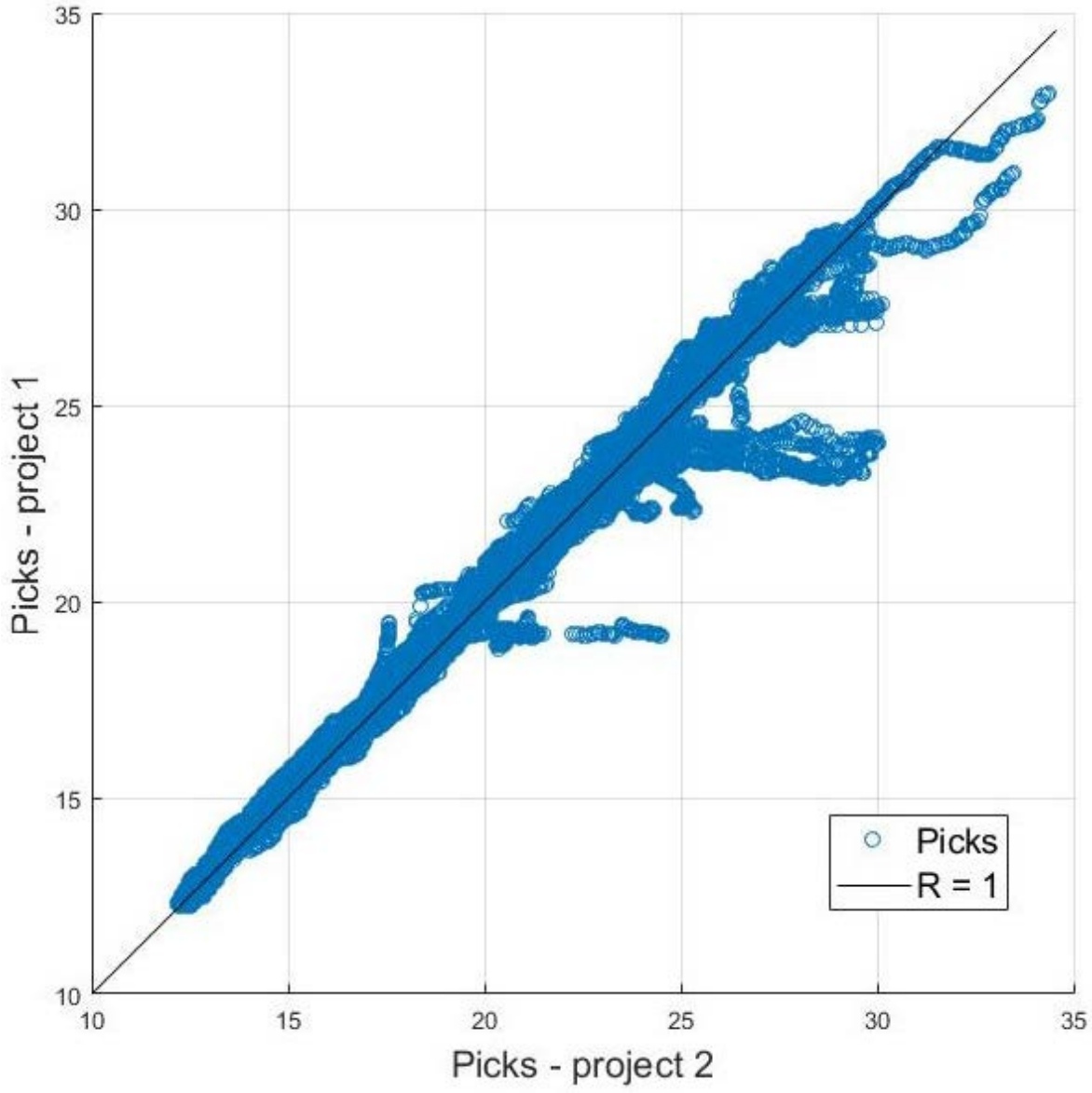

Figure 9. Correlation between the picks from the two sub-projects compared to a 100% positive correlation.

3.1 Water table variations

The depth to the water table in the study site is presented in Fig. 10. The depth to the water table is the same as the ice thickness between the surface and the water table. Note that the measurements do not all come from the same year. The background for Fig. 10–14 show surface topography expressed in terms of steepness of the slopes, where lighter colours indicate gentler slopes and darker colours indicate steeper slopes.

A slight NNW–SE trend can be observed. Although not entirely homogeneous, the water table is deeper in the NNW parts of the area, ~19–32 m, while it is shallower in the SE parts, ~14 m. The largest depth to the water table is 32.97 m while the smallest depth is 12.21 m. It can be observed that the shallowest depths are concentrated in the middle of the small grid of the GPR traces and in the NE-most part of the big grid of the GPR traces.

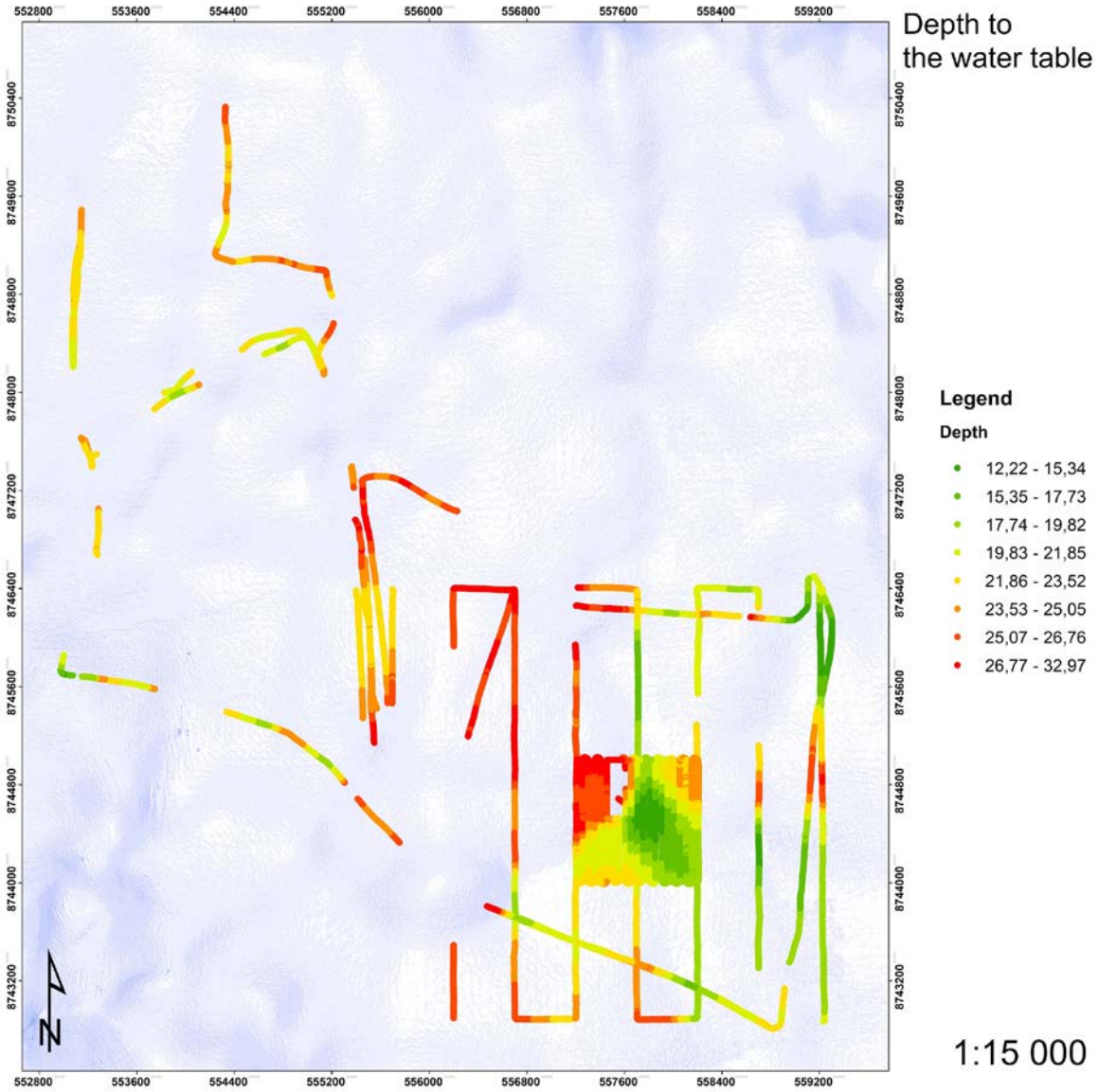

Figure 10. Depth to the water table (m). The shaded relief DEM in the background provided by ©Norwegian Polar Institute.

The hydraulic head in the study site is presented in Fig. 11. The map shows the absolute elevation at which the top of the water table is found calculated by subtracting the depth to the water table from the surface elevation. The darker blue colours indicate a deeper water table while lighter blue colours indicate a shallower water table. A distinct NNW–SE trend can be observed; the water table appears closer to the surface in the SE parts of the site and deeper in the NNW parts. This trend is also depicted by the arrows.

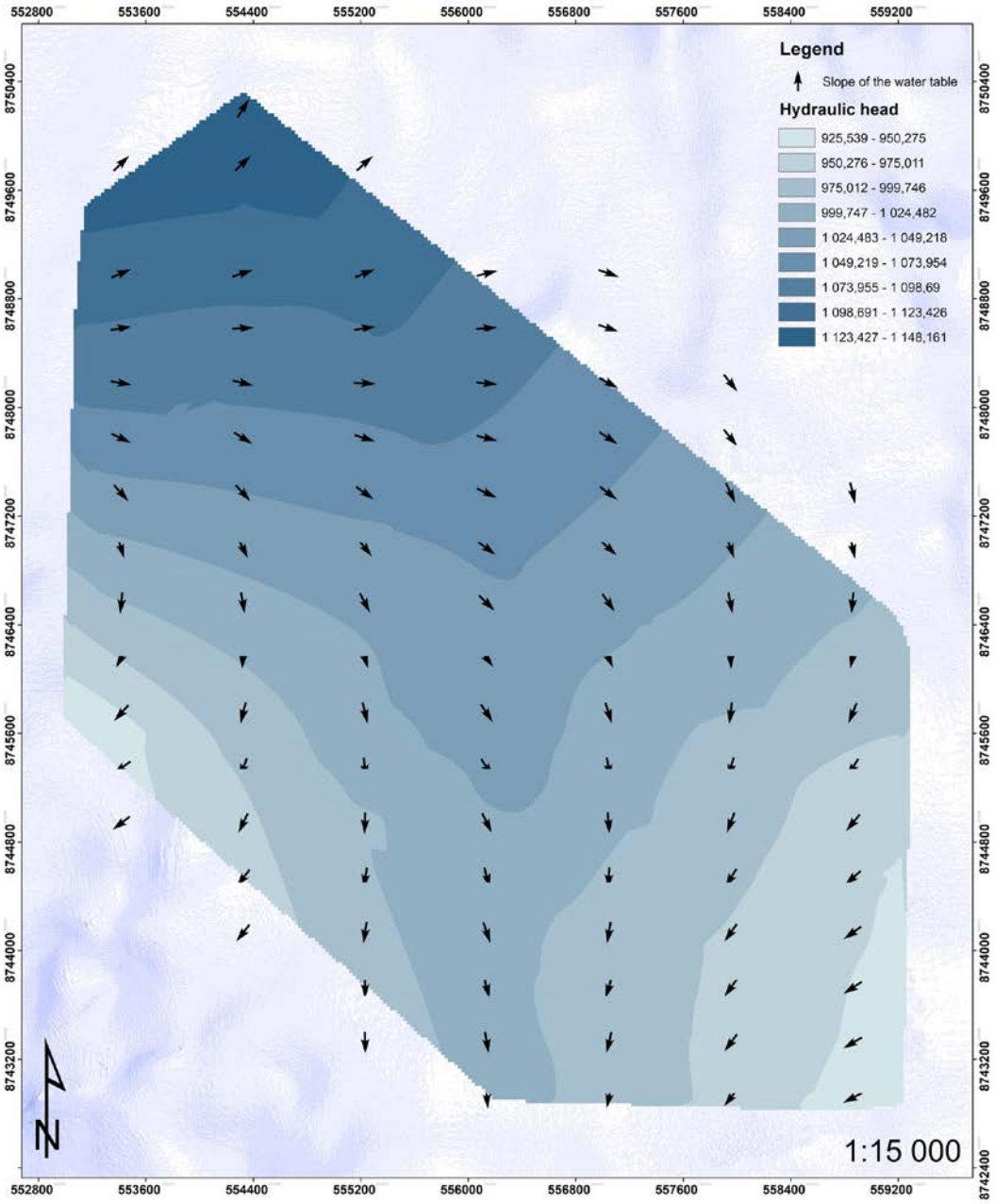

Figure 11: The interpolated values of hydraulic head that represent depth at which the water table is found (m). The black arrows show the direction of the water flow. The shaded relief DEM in the background provided by ©Norwegian Polar Institute.

Variations in depth to the water table in the intersection points between profiles from years 2015 and 2016 are presented in Fig. 12. The smallest change was 0.02 m while the biggest change was 1.4 m. The difference is calculated by comparing the earlier year (2015) with the latter year (2016). All numbers are positive, which means that in 2015 the depth to the water table was greater than in 2016.

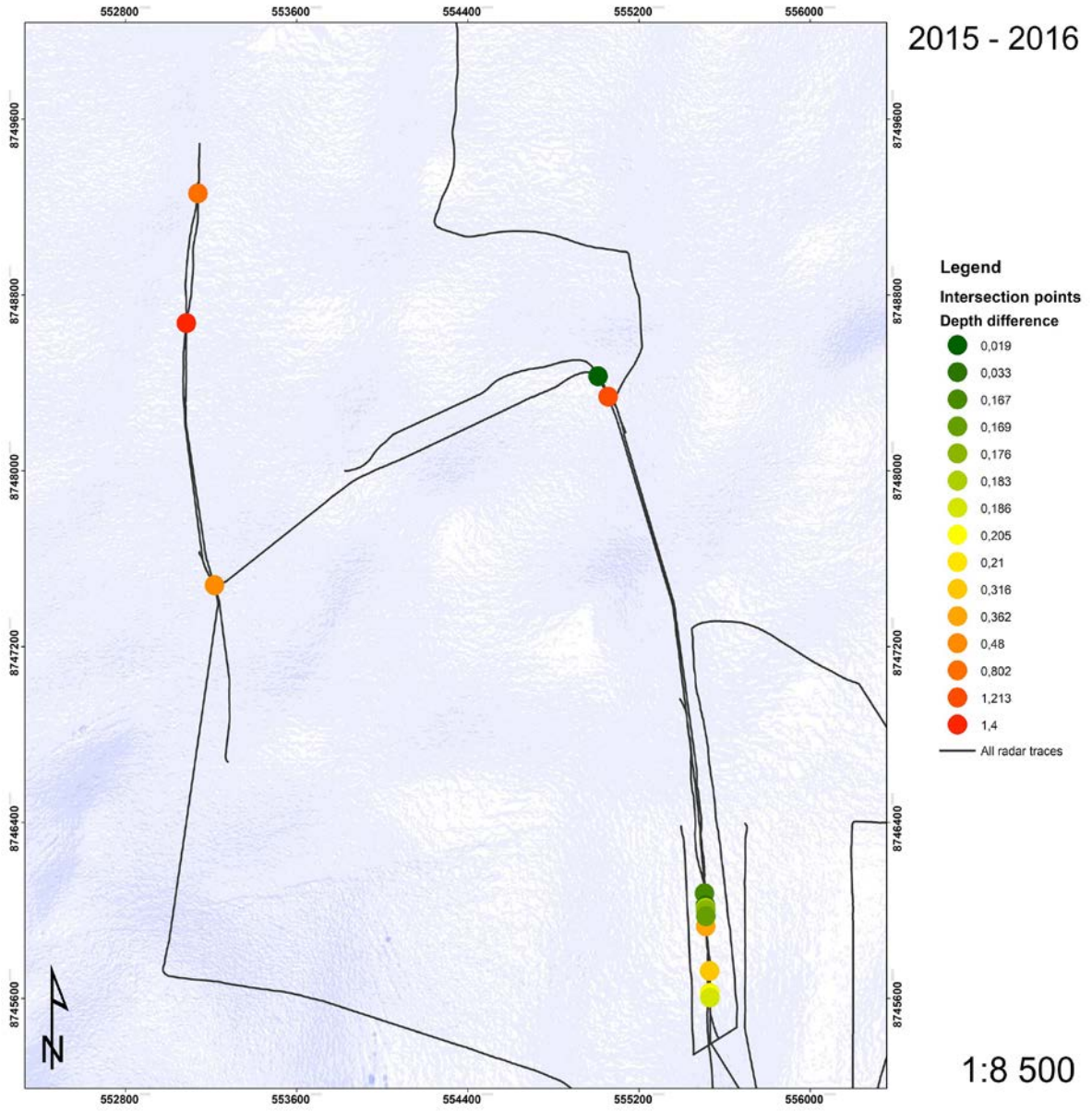

Figure 12. Variations in depth to the water table (m) between years 2015–2016 in intersection points between profiles from these years. The variations are expressed as difference between these two years, the difference is displayed on the Legend. The shaded relief DEM in the background provided by ©Norwegian Polar Institute.

Variations in depth to the water table in the intersection points between profiles from years 2016 and 2017 are presented in Fig. 13. The biggest differences of ~1 m can be observed in the NW part of the big grid. The numbers are positive, which means that in 2016 the depth to the water table was greater than in 2017.

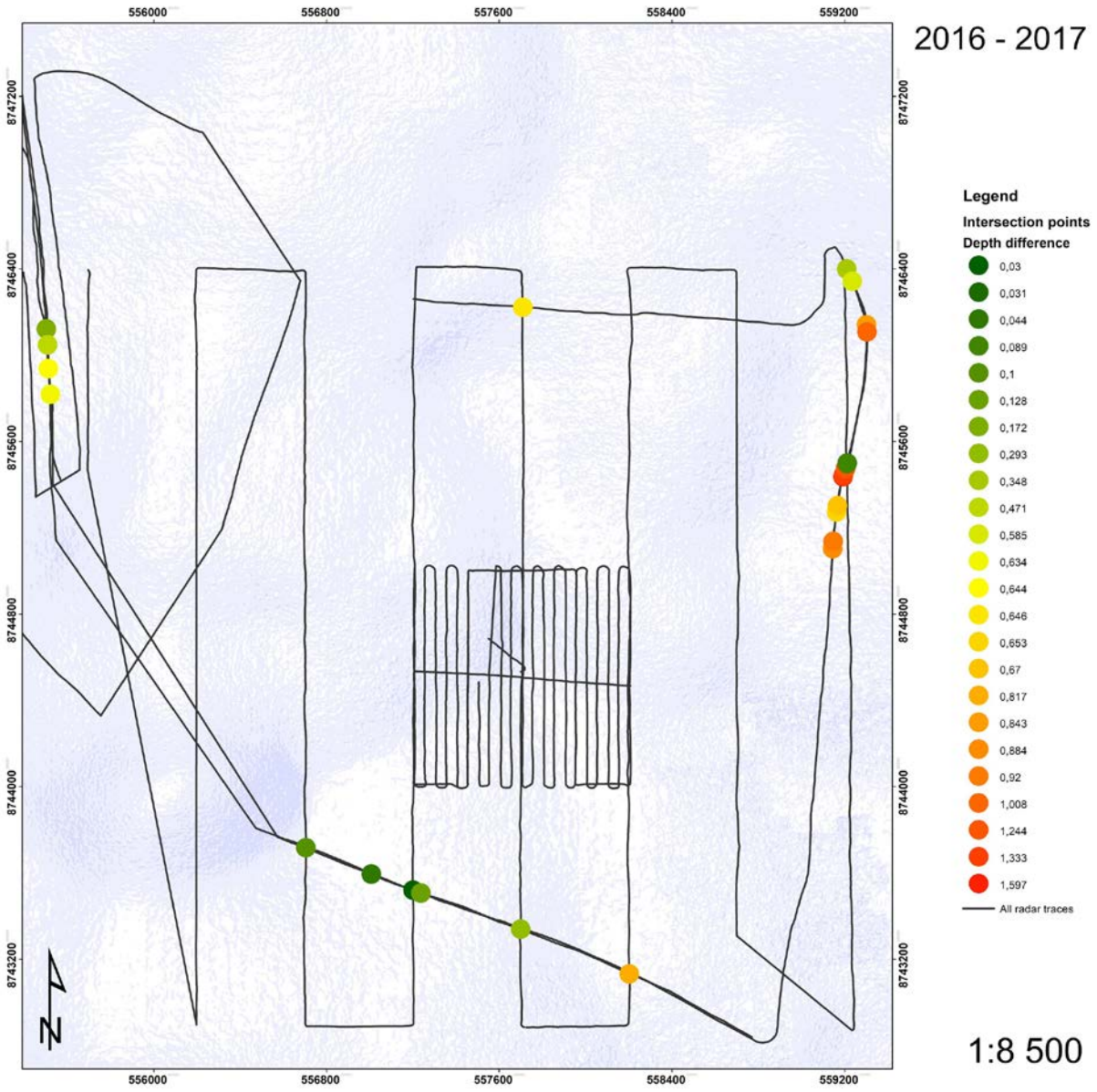

Figure 13. Variations in depth to the water table (m) between years 2016–2017 in intersections points between profiles from these years. The variations are expressed as difference between these two years, the difference is displayed on the Legend. The shaded relief DEM in the background provided by ©Norwegian Polar Institute.

Variations in depth to the water table in the intersection points between profiles from years 2017 and 2018 are presented in Fig. 14. The negative numbers indicate that the water table was closer to the surface in 2017 and deepened in 2018. Most of the numbers are positive, which means that in 2017 the depth to the water table was greater than in 2018. The biggest differences are concentrated in the middle of the small grid, ~1 m difference.

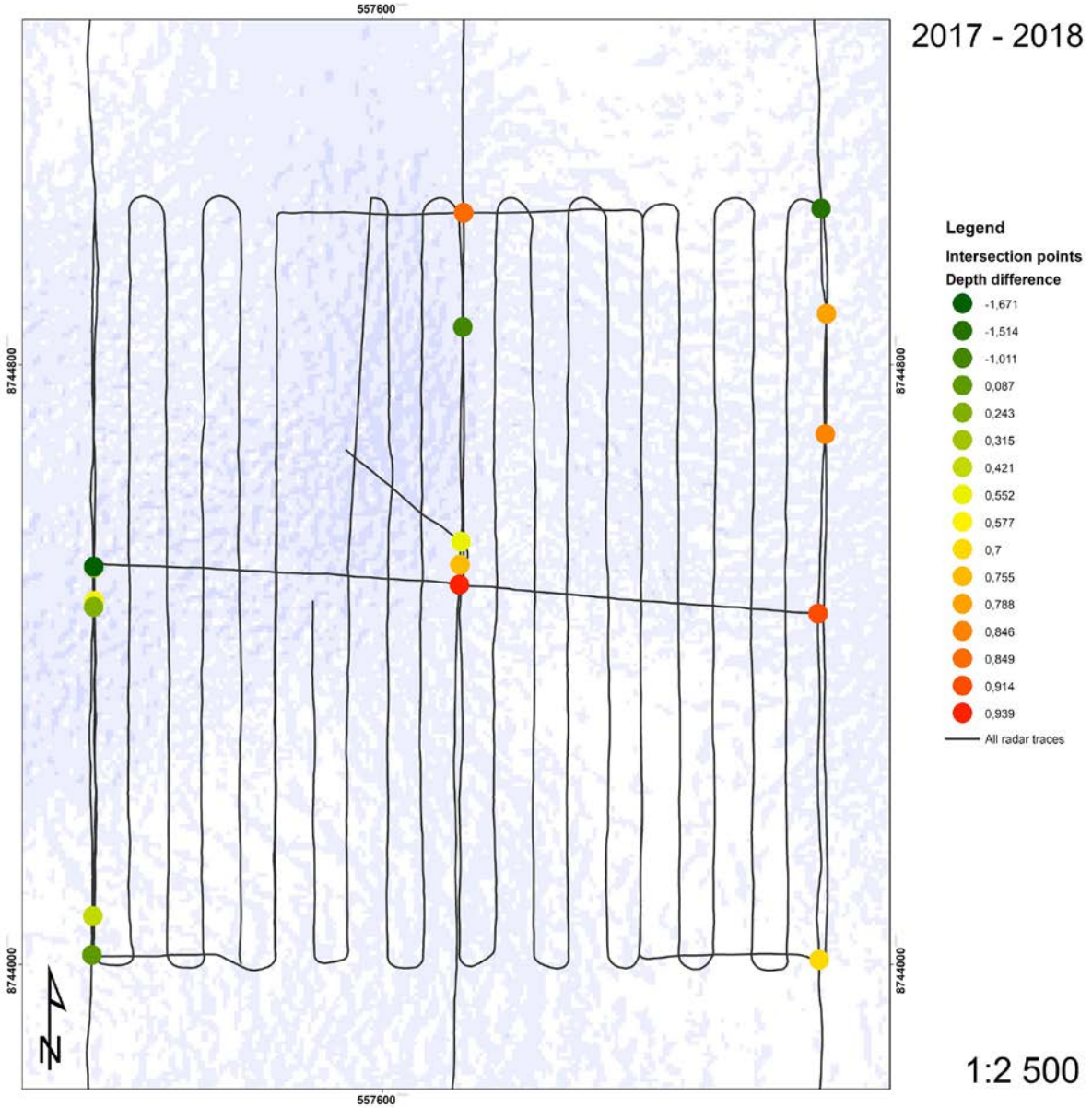

Figure 14. Variations in depth to the water table (m) between years 2017–2018 in intersections points between profiles from these years. The variations are expressed as difference between these two years, the difference is displayed on the Legend. The shaded relief DEM in the background provided by ©Norwegian Polar Institute.

Figure 15 shows the compiled average depth to the water table in the entire study site from the years 2015–2018. A clear declining trend can be observed. The average depth was 23.22 m in 2015, 22.26 m in 2016, 22.18 m in 2017 and 20.96 m in 2018. The average depth in the whole area is 22.16 m. The depth to the water table has overall decreased with 2.26 m from year 2015 to year 2018.

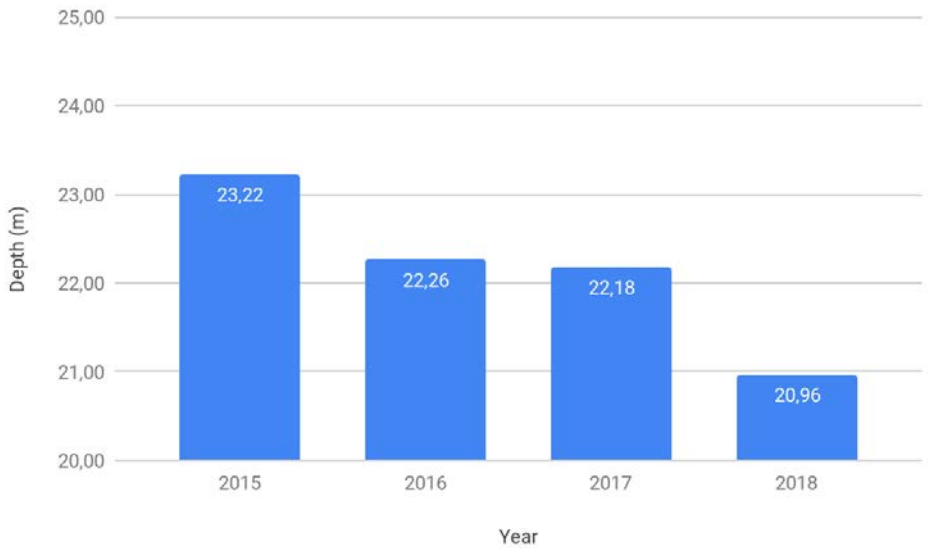

Figure 15. The average depth to the water table (m) in the study site over the four years.

3.2 Estimation of reflectivity

The results from the correlation between the reflectivity values and the slope of the water table, the surface topography slope, and the surface topography elevation are presented through histograms and scatter plots. The histograms (Fig. 17a-c) all consist of two overlapping datasets. The first dataset, named *All traces*, represents all the points where radar probing has been performed, regardless of whether a water table reflected the radar wave back or not. The second one, *Traces with reflections*, only represents the traces where there is water present in the firn aquifer. The overlapping traces can be seen in Fig. 16. In the histograms, the strength of the reflectivity is not taken into account, but the y-axis rather describes the number of points where a reflection from the water table was recorded.

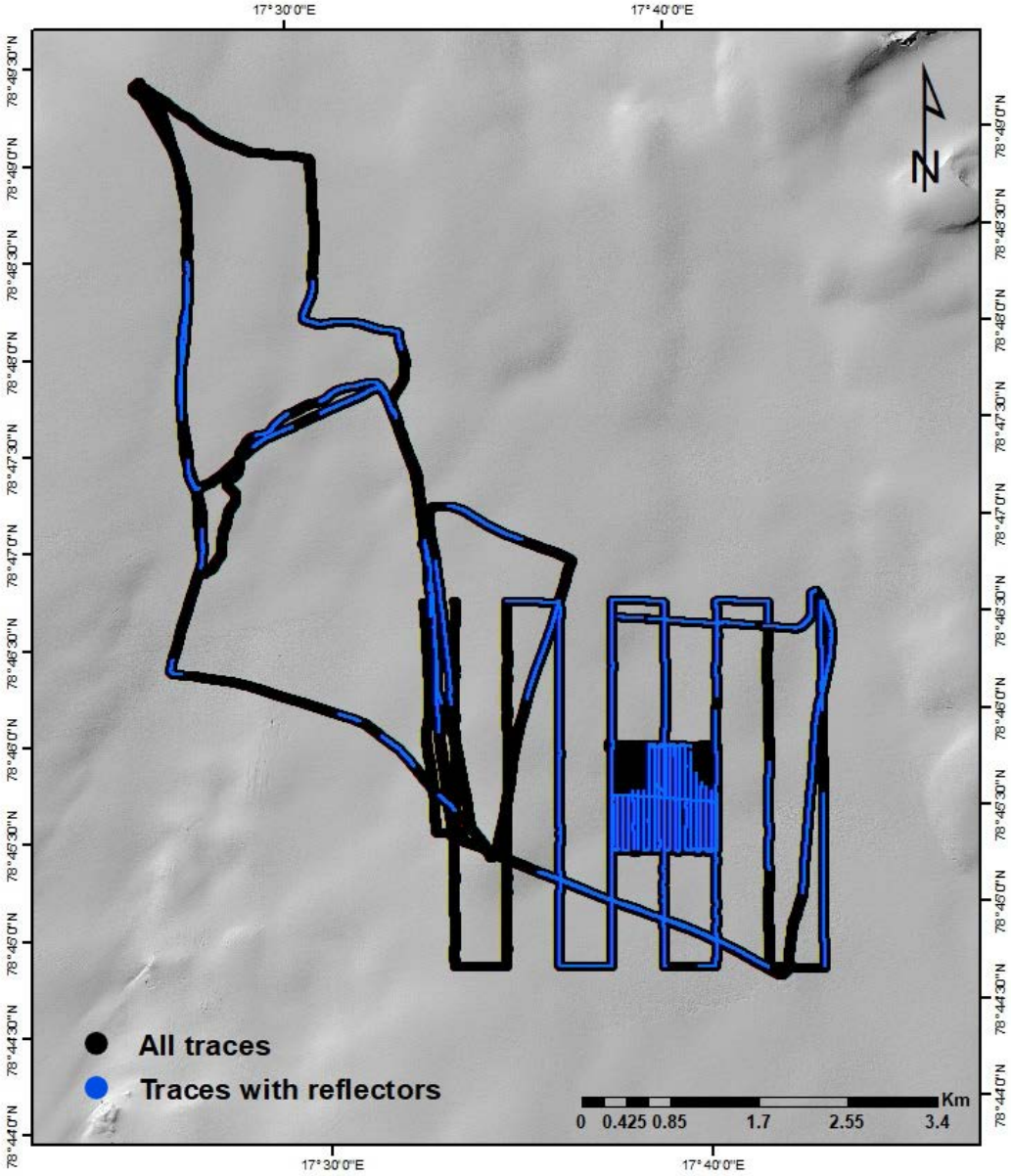

Figure 16. The traces from the GPR surveys, both with and without water table reflectors. The shaded relief DEM in the background provided by ©Norwegian Polar Institute.

The correlation of reflectivity against the slope of the water table shows that the radar probing was focused on areas where the slope of the water table lies between 1° and 2°, while there are very few points with a slope close to 0° and above 4° (Fig. 17a). The reflections from the top of the water table show a clear preference towards the gentle slopes. This is indicated by the fact that the dataset *Traces with reflectors* is skewed to the left; in slopes between 0° and 1° almost all points where the radar probing was performed have a returned reflection from the top of the water table whereas the more steep slopes have less points with reflections relative to the number of probings.

The slope of the surface topography in the study area lies between 0° and 12°, while the vast majority is below 6°. The reflectors from the water table are centred around a 2° slope (Fig. 17b). The two datasets *All traces* and *Traces with reflectors* follow each other very closely; the magnitude of the slope where the radar probing had few points also showed a low number of returned reflectors and the maximum value at circa 2° is true for both datasets.

The elevation in the area where the GPR was performed lies between 900 and 1,200 m a.s.l., with most of the points within the interval 960–1,075 m a.s.l. The return of the reflectors show that the water table mainly lies in areas with a relatively low elevation, more specifically lower than 1,000 m a.s.l. (Fig. 17c).

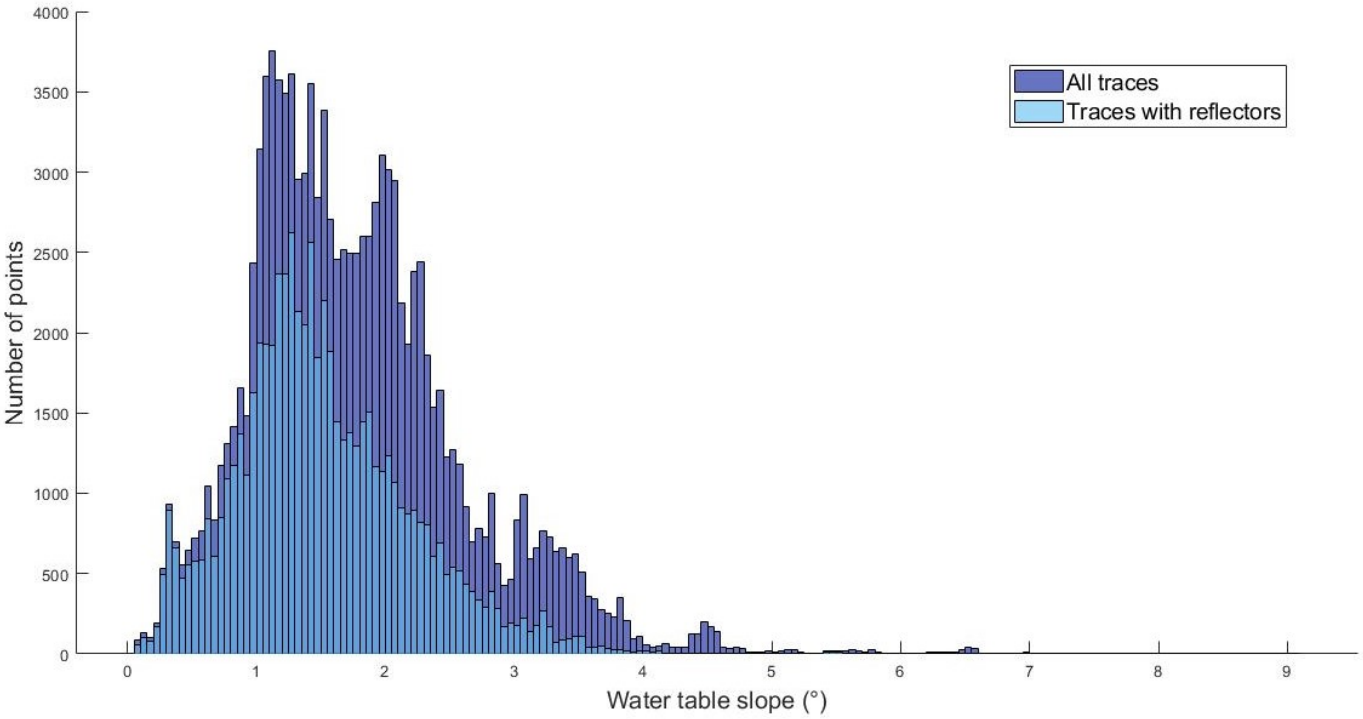

Figure 17a. The correlation between reflectivity and slope of the water table. The reflectivity is denoted as number of points. The darker bars represent all traces from the GPR in the research area, while the lighter blue bars show the water table reflectors.

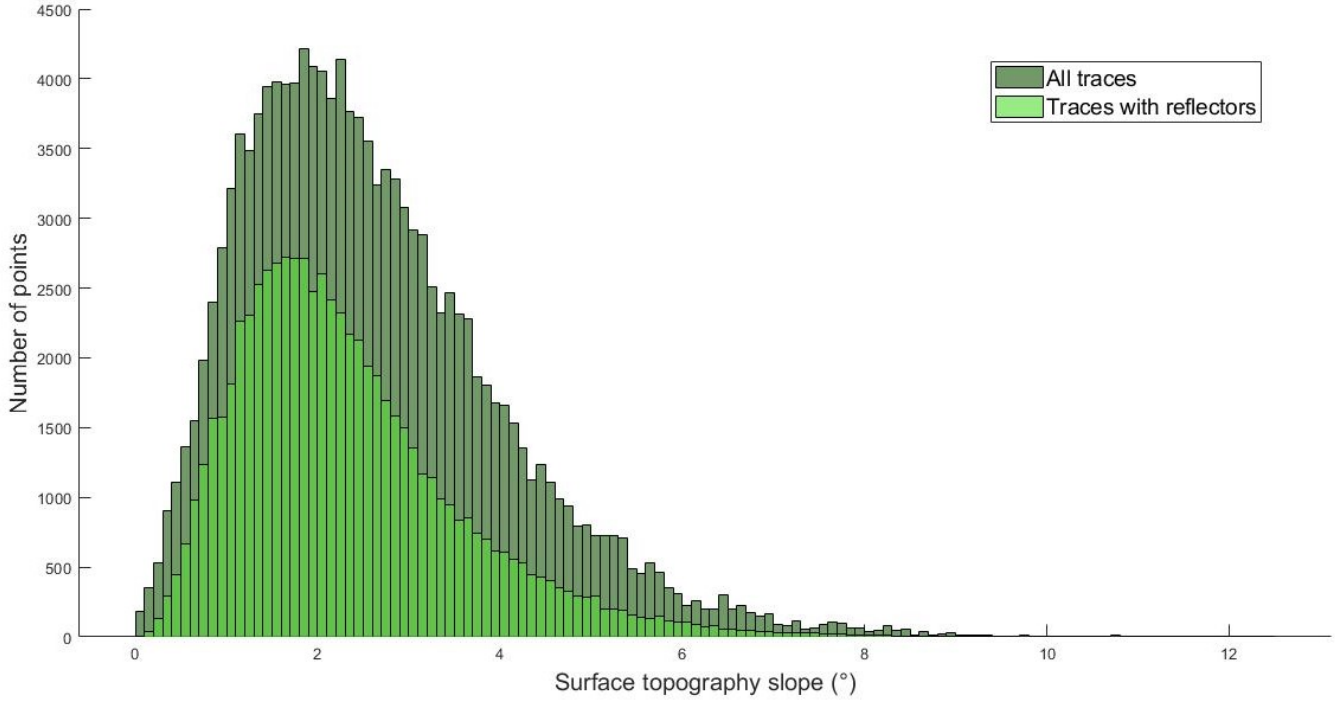

Figure 17b. The correlation between reflectivity and slope of the surface topography. The dark green bars represent all traces from the GPR in the research area, while the lighter bars represent points where the water table is found.

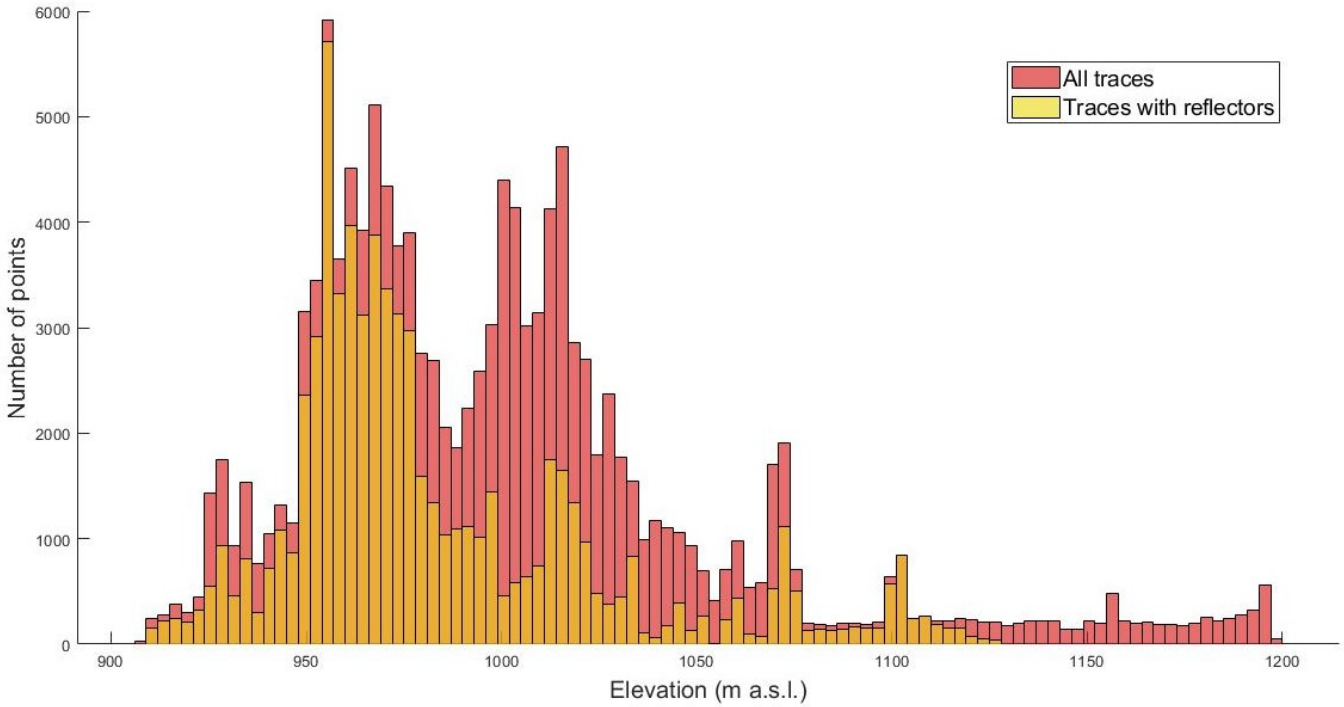

Figure 17c. The correlation between reflectivity and surface elevation. The red bars show the elevation where the radar analysis was performed, and the yellow bars represent the elevation in the areas where the water table exists.

Scatter plots representing the magnitude of reflectivity versus water table slope show a slight negative trend, i.e. areas with a steeper slope have a weaker water table reflectivity (Fig. 18a). The same trend is found in the correlation between reflectivity and surface topography slope (Fig. 18b). For the water table slope, the trendline is fitted to the maximum reflectivity values whereas for the surface topography slope the trendline is fitted to the 0.3% highest reflectivity values.

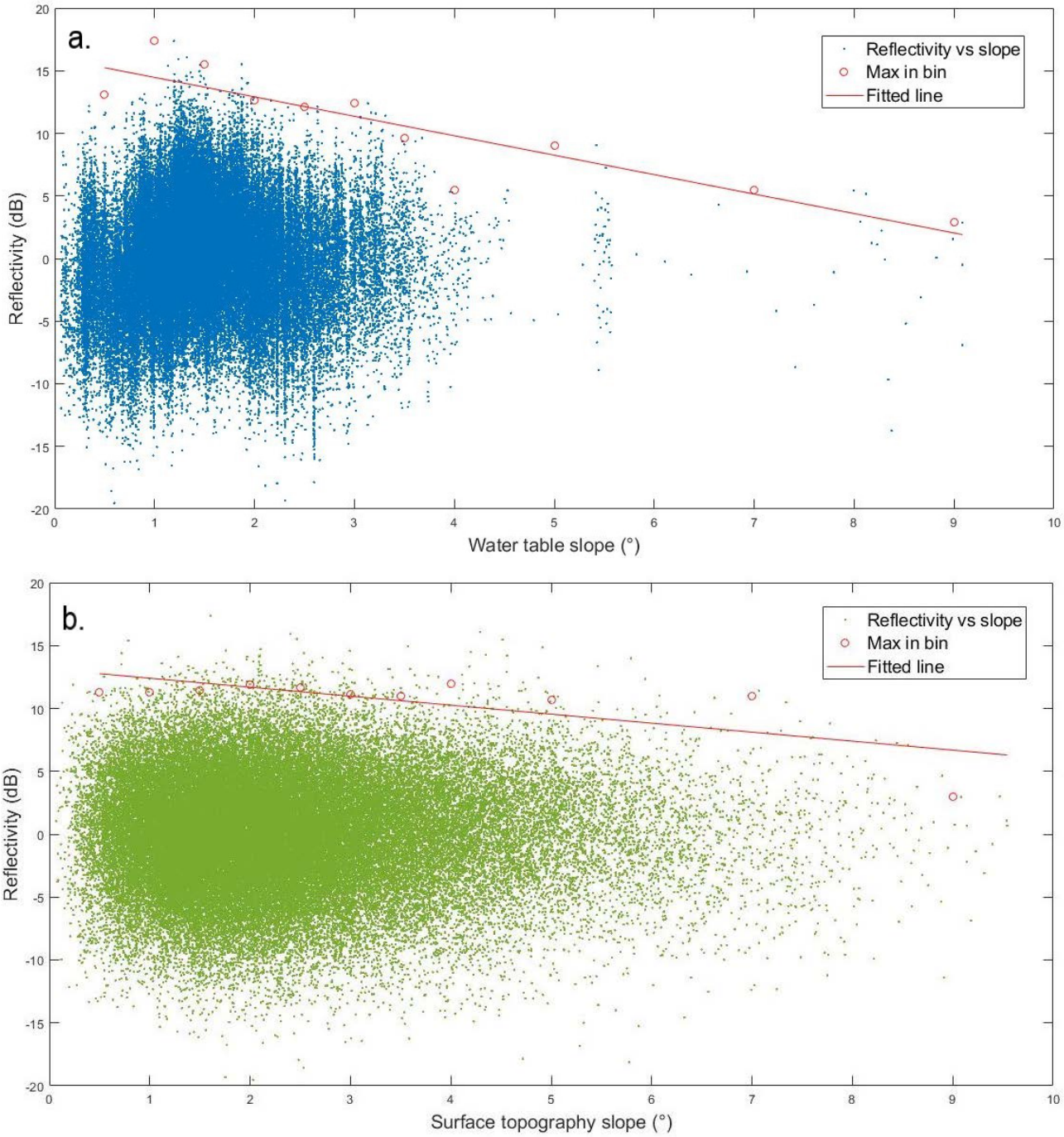

Figure 18. Strength of reflectivity over different slope angles in a) the water table and b) the surface topography. Linear fits to the data show a negative trend, i.e. stronger reflectivity in steeper slopes.

4. Discussion

4.1 Water table variations

It is important to keep in mind that the radar measurements that are the basis for the analysis of the PFA in this thesis are not all taken during the same year or repeated at the same places. However, the factors inducing movement of the water (gravity, hydraulic gradient) are always present. It is therefore plausible that in the NNW part of the study site the depth at which water table is present will always be greater than that depth in the SE part. Consequently, the results are deemed as representative for the aquifer and are still regarded as valid.

Depth to the water table varies considerably between different years and especially between the different parts of the study site, as displayed in Fig. 12–14. On all these maps, the values were calculated by subtracting the depth value of the latter year from the value of the previous year. Most of the values are positive numbers which means that overall, the water table was rising in the area from year to year. One conclusion could be that the supply of water exceeds the discharge. This could mean that the aquifer either drains very slowly or does not drain and instead accumulates water until a threshold is reached and the water is released in a sudden event. Considering the first possibility, it is plausible that the aquifer has not yet developed a hydrological system that would allow an unhindered continuous discharge. It could mean that the aquifer is a rather young feature and such a system has not developed yet.

There appears to be only three points where depth to the water table increased between 2017 and 2018. All three points are in areas with slightly higher topography and steeper slopes. Since it is only three seemingly not correlated points, it is plausible that it was caused by local factors.

It is very clear that the depth to the water table decreases each year of the study, as seen in Fig. 15. The most substantial difference occurs between the years 2017 and 2018. This implies that the water table rose slowly but steadily 2015–2017 (~0.5–1 m) and then rose considerably more 2017–2018 (~2.6 m). There can be many reasons for this sudden rise to happen. One possible explanation is an exceptionally warm melt season. High melt rates imply more meltwater that can fill the aquifer. However, another consequence of high melt rates is lowering of the surface elevation. This means that the glacier’s surface is lowered towards the water table. Another factor affecting the surface topography is the flow of ice. In the study site, due to the mostly prevalent shallow slopes, the flow of ice can be expected to be very slow and inertial enough to not reflect the annual mass changes. Another reason for a rise of the water table could be low accumulation rates. High melt rates and low accumulation rates mean lowering of the surface of the glacier which in turn decreases the distance to the water table. However, we lack data to prove these theories. A more detailed analysis of the GPS data from the radar profiles might provide some insight into the extent of the surface lowering.

There seems to be a correlation between angle of the surface slope and depth to the water table as well as the surface elevation (expressed as hydraulic head in Fig

11). They all seem to follow the NNW–SE trend. It can be concluded that the water table surface follows patterns in the surface elevation, i.e. higher surface elevation correlates to a deeper water table while low surface elevation correlates to a shallower water table. The results show also a clear connection between areas with gentle slopes and shallow water table while steeper slopes are mainly associated with deeper water table.

The entire area of the study site is dominated by rather gentle surface slopes. Such slopes are associated with low topographic points as described by Christianson *et al*. (2015). Especially gentle slopes can be observed around the small grid (e.g. Fig. 10) which also coincides with a topographic depression. Moreover, the depth to the water table is considerably greater in the NNW parts of the area than in the SE parts (Fig. 10). The water table appears to be closest to the surface in the middle of the small grid (~12 m), which is plausible considering that the preferred water movement is from high hydraulic potential to low and, consequently, from high terrain to low terrain. It can therefore be concluded that water flows towards the small grid area and gathers there, raising the water table surface closer to the glacier surface. What is interesting is that, theoretically, water should gather in the lowest part of the terrain. In the study area, the lowest elevation is even more towards SE (Fig. 11). However, our data clearly shows that the water table lies a few meters deeper in that area than in the small grid. It is thus possible that water that gathers in the middle of the small grid is still while water in SE part of the area is in motion. This could be supported by the fact that the surface elevation of the area in the direct proximity to this small grid is slightly higher, which also correlates to slightly deeper water table. It is therefore speculated that in that sheltered place there is a bowl-like hollow in the firn that allows water to gather and be still.

4.2 Estimation of reflectivity

4.2.1 Reflectivity dependence on water table slope

The reflections from the water table are mainly distributed in areas with gentler slopes (Fig. 17a). A steeper surface topography leads to a more rapid water flow and the slope of the water table is supposedly steep where the surface topography is steep (Christianson *et al.*, 2015), meaning that in our areas with a steeper water table slope the water flows faster. This leads to a distribution of the flowing water in the firn, which in turn results in a more diffuse reflection from the top of the saturated zone. If the flow is very high, the reflection may be completely lost. This theory is further consolidated by the scatter plot (Fig. 18a). The trendline fitted to the maximum reflectivity values is negative, meaning that that the reflectivity values are smaller in the areas where the slope is steeper.

4.2.2 Reflectivity dependence on surface topography slope

The water table reflectors are clustered around a surface topography slope of about 2°, with the majority of the reflectors found below 6°. According to Christianson *et al.* (2015), a steeper slope of the surface topography leads to a more rapid flow of water, which in turn thins the saturated firn zone. This leads to the water flowing towards

areas with a gentler slope, where it accumulates. This results in the water table being more frequently detected by the radar in areas where the surface slope is gentle. Since the result shows that the water table reflectors have a clear preference towards the less steep slopes, it could indicate that this theory is true for the Lomonosovfonna firn aquifer. However, the traces containing reflections follow the dataset containing *All traces* very closely (Fig. 17b). It might therefore be argued that the preference from the reflectors towards gentle slopes only represents the overall distribution of traces. When the area that is being investigated mainly has more gentle slopes, it is also more likely that the traces which show reflections also lie within the boundaries of gentle slopes. This might implicate that the aforementioned conclusion is based on very weak evidence. However, the conclusion might be strengthened slightly by Fig. 18b. It shows that a stronger reflectivity is found where the slopes are gentler which indicates the presence of more water in the firn in these gentler slopes.

4.2.3 Reflectivity dependence on elevation

The data distribution of the *All traces* is larger than the data distribution of the dataset containing the reflection traces. This implies that the concentration of the water table reflections in areas with an elevation around 1,000 m a.s.l. is truly derived from the fact that lower elevations are preferential for the water table. A possible explanation could be that a lower elevation generates more meltwater, which can percolate down and fill the pore space in the firn, leading to a stronger reflection from the top of the water-saturated firn.

4.3 Joint discussion

The picking of the water table was done manually, introducing a source of error due to human bias. To acknowledge this, the picking done in the two different projects was compared and the correlation coefficient and standard deviation was calculated (Fig. 8). The correlation coefficient ($R = 0.9923$) was very close to 1, which represents a perfect positive correlation. The standard deviation ($\sigma = 0.45$) was relatively small. With these two values considered, the conclusion is that the picking for the two different projects was very similar and the human bias did not introduce a large error to the results. However, at a couple of places the picks deviated quite a lot from each other. A plausible reason for this is that a couple of the radar profiles had very weak reflections from the top of the water table in some places. If one decided that there was a water table when the other didn't, the picking might turn out to be very different in those profiles, introducing a larger error.

Comparison of project 1 and project 2 shows that there is in fact a correlation of the presence of the water table and the surface slopes and the slopes of the water table. The strong reflections seem to be mostly in the areas with gentle slopes and the reflections are considerably vaguer in the areas with steeper slopes. This corresponds well with the dynamics of water flow. It is speculated that no or unremarkably little water movement takes place in the gentle sloped areas which would mean that the reflected signal is much stronger and easier to detect with radar.

Because water flows from high to low hydraulic potential, which is also correlated to slopes, water flow will occur in the areas with steeper slopes which would also lead to scattered reflection and therefore weaker signal.

Our results seem to agree with the results of the research on Holtedahlfonna ice field, which in turn are similar to the results of aquifer research on Greenland (Christianson *et al.*, 2015). Our data proved that the most water-saturated part of the Lomonosovfonna firn aquifer forms in the slight depression in the glacier, similarly to the aquifer found in Holtedahlfonna.

Since measurements of accumulation rates and melt rates in our study site are lacking, it is hard to draw any fact-based conclusions concerning the reason why the water table rose so drastically between 2017 and 2018 and if there are other factors affecting the distribution of water as shown by the reflectivity. This could be considered an area of improvement and a good starting point for future research on Lomonosovfonna would be the method *inverse estimation of accumulation* as explained by Van Pelt *et al.* (2014). In the summer, densification of the upper layer of the glacier occurs in the accumulation zone, which would be represented by high reflectivity in ground penetrating radar profiles. The resulting layering in the radar profiles can then be used to estimate the accumulation variability. Additionally, coupled models can estimate e.g. surface melt, percolation, and runoff (Van Pelt *et al.*, 2014)**.**

5. Conclusions

Water movement through firn in a glacier is determined by gradients in the hydraulic potential and is correlated to surface topography as well as steepness of the surface slopes. Water flows towards low topographic points with gentle slopes and gathers there creating standing bodies of water. High topography and steep slopes induce flow of water towards lower topographic points. The depth to the water table in the PFA in Lomonosovfonna varies with time, rising closer to the surface during the four years. The reflectivity analysis confirms the hypothesis regarding where water gathers and where it flows. The spatial and temporal variations in the roof of the water table are confirmed by both projects.

Contributions

Monika Hawrylak worked with Project 1 and wrote the following sections: Objective, Glacial hydrology, and Radar.
Emma Nilsson worked with Project 2 and wrote the following chapters: Glaciers, Ground penetrating radar, and Site description.
Both students contributed to the following chapters: Previous studies on perennial firn aquifers, Method, Results, Discussion, and Conclusions.

Acknowledgements

We would like to thank our supervisors, Sergey Marchenko and Rickard Pettersson, for the valuable feedback on the different stages of this thesis as well as the enormous help with understanding the data and solving technical problems. Monika Hawrylak would like to thank Jakob Berndtsson for proofreading, encouragement and technical help.

References

Benn, D.I. & Evans, D.J.A. (2010). *Glaciers & glaciation*. 2nd ed. London: Routledge.

Bennett, M. & Glasser, N.F. (2009). *Glacial geology: ice sheets and landforms*. 2nd ed. Chichester, UK & Hoboken, NJ: Wiley-Blackwell.

Christianson, K., Kohler, J., Alley, R.B., Nuth, C. & Pelt, W.J.J. van (2015). Dynamic perennial firn aquifer on an Arctic glacier. *Geophysical Research Letters*, vol. 42 (5), pp. 1418–1426.

IPCC (2013) *Climate change 2013: The Physical Science Basis. Contribution of Working Group I to the Fifth Assessment Report of the Intergovernmental Panel on Climate Change* [Stocker, T.F., D. Qin, G.-K. Plattner, M. Tignor, S.K. Allen, J. Boschung, A. Nauels, Y. Xia, V. Bex, P.M. Midgley (eds.)]. Cambridge University Press, Cambridge, United Kingdom and New York, NY, USA.

Koenig, L.S., Miège, C., Forster, R.R. & Brucker, L. (2014). Initial in situ measurements of perennial meltwater storage in the Greenland firn aquifer. *Geophysical Research Letters*, vol. 41 (1), pp. 81–85.

Kuipers Munneke, P., Ligtenberg, S.R.M., Broeke, M.R. van den, Angelen, J.H. van & Forster, R.R. (2014). Explaining the presence of perennial liquid water bodies in the firn of the Greenland Ice Sheet. *Geophysical Research Letters*, vol. 41 (2), pp. 476–483.

Miège, C., Forster, R.R., Brucker, L., Koenig, L.S., Solomon, D.K., Paden, J.D., Box, J.E., Burgess, E.W., Miller, J.Z., McNerney, L., Brautigam, N., Fausto, R.S. & Gogineni, S. (2016). Spatial extent and temporal variability of Greenland firn aquifers detected by ground and airborne radars. *Journal of Geophysical Research: Earth Surface*, vol. 121 (12), pp. 2381–2398.

Miller, O., Solomon, D.K., Miège, C. & Koenig, L. (2018). Direct Evidence of Meltwater Flow Within a Firn Aquifer in Southeast Greenland. *Geophysical Research Letters*, vol. 45 (1), pp. 207–215.

Plewes, L.A. & Hubbard, B. (2001). A review of the use of radio-echo sounding in glaciology. *Progress in Physical Geography; London*, vol. 25 (2), pp. 203–236.

Poinar, K., Joughin, I., Lilien, D., Brucker, L., Kehrl, L. & Nowicki, S. (2017). Drainage of Southeast Greenland Firn Aquifer Water through Crevasses to the Bed. *Frontiers in Earth Science*, vol. 5. DOI: https://doi.org/10.3389/feart.2017.00005.

Van Pelt, W.J.J., Oerlemans, J., Reijmer, C.H., Pohjola, V.A., Pettersson, R. & Angelen, J.H. van (2012). Simulating melt, runoff and refreezing on Nordenskiöldbreen, Svalbard, using a coupled snow and energy balance model. *The Cryosphere*, vol. 6 (3), pp. 641–659.

Van Pelt, W.J.J., Pettersson, R., Pohjola, V.A., Marchenko, S., Claremar, B. & Oerlemans, J. (2014). Inverse estimation of snow accumulation along a radar transect on Nordenskiöldbreen, Svalbard. *Journal of Geophysical Research: Earth Surface*, vol. 119 (4), pp. 816–835.

Van Pelt, W.J.J., Pohjola, V.A., Pettersson, R., Ehwald, L.E., Reijmer, C.H., Boot, W. & Jakobs, C.L. (2018). Dynamic Response of a High Arctic Glacier to Melt and Runoff Variations. *Geophysical Research Letters*, vol. 45 (10), pp. 4917–4926.

Internet resources

Koenig, M. (submitter); Koenig, M., Nuth, C. (analysts). (2010). *GLIMS Glacier Database*. Boulder, CO. National Snow and Ice Data Center. http://dx.doi.org/10.7265/N5V98602 [2019-04-11]

Norwegian Meteorological Institute (no date) http://sharki.oslo.dnmi.no [2019-04-16]

Norwegian Polar Institute (2014), *Terrengmodell Svalbard (Delmodell 5m 2011_25161_33*). Norwegian Polar Institute. https://doi.org/10.21334/npolar.2014.dce53a47 [2019-04-11]

Software

ESRI (2018) *ArcGIS Desktop* Version 10.6.1 Available at: http://desktop.arcgis.com/en/arcmap/

MathWorks (2018) *MATLAB* Version R2018b Available at: https://se.mathworks.com/?s_tid=gn_logo

S. ACADEMIE
ATIAE
RITAS